AD-A132 110 PRELIMINARY REPORT ON UVDEP AND PRODEP RESULTS FOR THE NRL (NAVAL RESEARC..(U) NAVAL RESEARCH LAB WASHINGTON DC E HYMAN ET AL. 16 AUG 83 NRL-MR-5146 1/1

UNCLASSIFIED F/G 18/3 NL

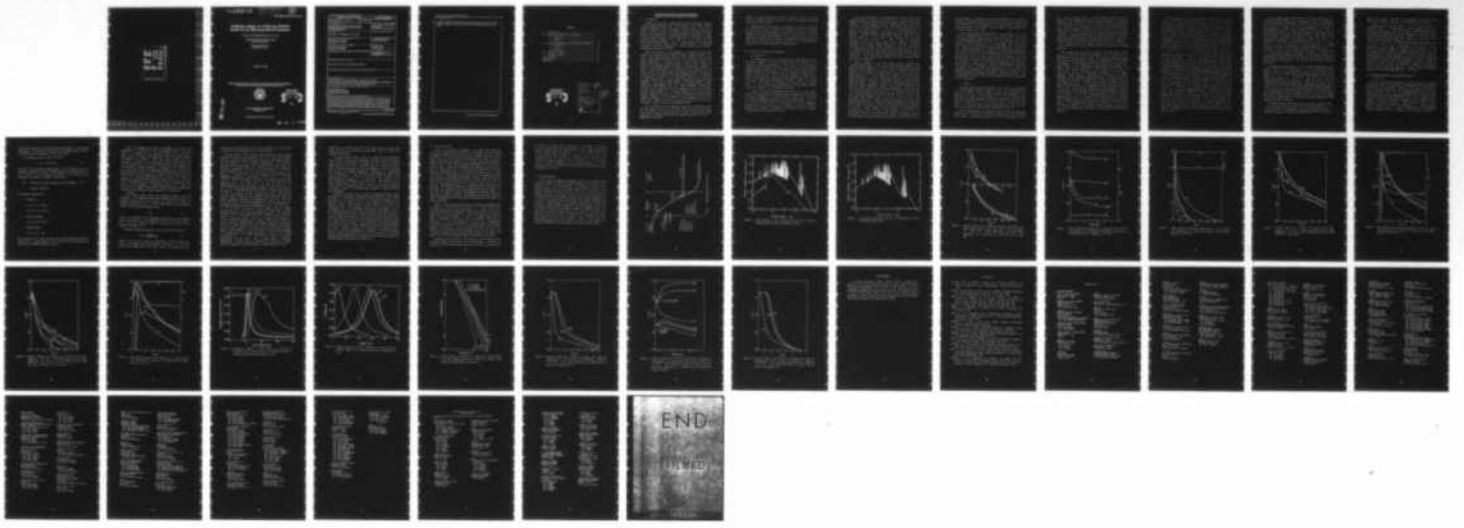

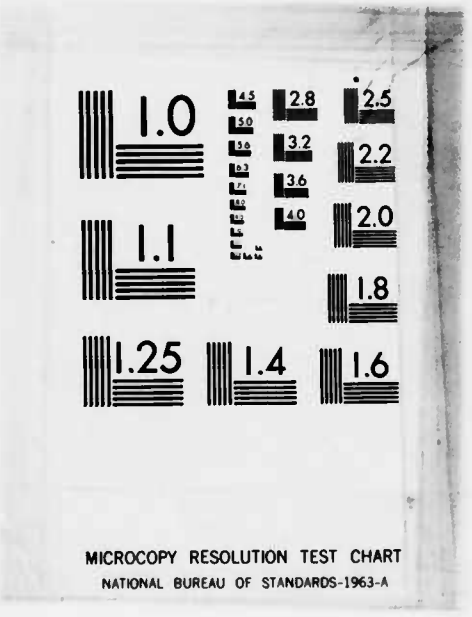
1.0
1.1
1.25
1.4
1.6
1.8
2.0
2.2
2.5
2.8
3.2
3.6
4.0
4.5
5.0
5.6
6.3
MICROCOPY RESOLUTION TEST CHART
NATIONAL BUREAU OF STANDARDS-1963-A

(2)

NRL Memorandum Report 5146

Preliminary Report on UVDEP and PRODEP Results for the NRL Laser/HANE Experiment

E. HYMAN,* M. MULBRANDON AND J. D. HUBA

Geophysical and Plasma Dynamics Branch
Plasma Physics Division

**Science Applications, Inc.*
McLean, VA 22102

August 16, 1983

This research was sponsored by the Defense Nuclear Agency under Subtask S99QMXBC, work unit 00067, and work unit title "Plasma Structure Evolution."

NAVAL RESEARCH LABORATORY
Washington, D.C.

SECURITY CLASSIFICATION OF THIS PAGE (When Data Entered)

REPORT DOCUMENTATION PAGE		READ INSTRUCTIONS BEFORE COMPLETING FORM
1. REPORT NUMBER NRL Memorandum Report 5146	2. GOVT ACCESSION NO. AD-A132110	3. RECIPIENT'S CATALOG NUMBER
4. TITLE (and Subtitle) PRELIMINARY REPORT ON UVDEP AND PRODEP RESULTS FOR THE NRL LASER/ HANE EXPERIMENT		5. TYPE OF REPORT & PERIOD COVERED Interim report on a continuing NRL problem. 6. PERFORMING ORG. REPORT NUMBER
7. AUTHOR(s) E. Hyman,* M. Mulbrandon and J.D. Huba		8. CONTRACT OR GRANT NUMBER(s)
9. PERFORMING ORGANIZATION NAME AND ADDRESS Naval Research Laboratory Washington, DC 20375		10. PROGRAM ELEMENT, PROJECT, TASK AREA & WORK UNIT NUMBERS 62715H; 47-0889-0-3
11. CONTROLLING OFFICE NAME AND ADDRESS Defense Nuclear Agency Washington, DC 20305		12. REPORT DATE August 16, 1983 13. NUMBER OF PAGES 45
14. MONITORING AGENCY NAME & ADDRESS(if different from Controlling Office)		15. SECURITY CLASS. (of this report) UNCLASSIFIED 15a. DECLASSIFICATION/DOWNGRADING SCHEDULE

16. DISTRIBUTION STATEMENT (of this Report)

Approved for public release; distribution unlimited.

17. DISTRIBUTION STATEMENT (of the abstract entered in Block 20, if different from Report)

18. SUPPLEMENTARY NOTES

*Present address: Science Applications, Inc., McLean, VA 22102

This research was sponsored by the Defense Nuclear Agency under Subtask S99QMXBC, work unit 00067, and work unit title "Plasma Structure Evolution."

19. KEY WORDS (Continue on reverse side if necessary and identify by block number)

Laser HANE simulation
Collisional effects (coupling)
Radiation effects (ionization)

20. ABSTRACT (Continue on reverse side if necessary and identify by block number)

We present predictions for the NRL laser/HANE experiment of the effects on an N_2 background gas of (1) x-rays emitted following laser irradiation of an aluminum target, (2) debris ions moving out from the target, and (3) deposition of uv radiation resulting from interaction between the debris ions and the background gas. We calculate both primary ionization and time dependent chemistry changes. Results are based on two NRL codes, UVDEP and PRODEP, developed for HANE studies. Certain assumptions

(Continues)

DD FORM 1 JAN 73 1473 EDITION OF 1 NOV 65 IS OBSOLETE
S/N 0102-014-6601

SECURITY CLASSIFICATION OF THIS PAGE (When Data Entered)

20. ABSTRACT (Continued)

made in the codes are uncertain and/or violated to some extent within the context of the NRL experiment. Hence, the results must be considered preliminary and first order.

CONTENTS

PRELIMINARY REPORT ON UVDEP AND PRODEP RESULTS FOR THE NRL LASER/HANE EXPERIMENT

I. Introduction

Recently, there has been renewed interest in the laboratory simulation of HANE phenomena (Vesecky et al., 1980; Cornwall et al., 1981). DNA is presently sponsoring a major experiment at NRL in which a laser beam is used to "explode" a target. The subsequent interaction between the target plasma and the ambient gas in the target chamber is believed to be similar to the interaction between a weapon's debris and the atmosphere in certain parameter domains (Longmire et al., 1981; Tsai et al., 1982; Smith and Huba, 1983; Sperling, 1983). Thus, an understanding of the phenomena occurring in the laser experiment may provide insight into the physical processes and consequences of HANE.

One of the purposes of the experiment is to study the collisionless coupling of the debris and air plasma via plasma turbulence (Lampe et al., 1975). This coupling mechanism relies upon the excitation of one or more plasma instabilities in the debris shell. The fluctuating electric and magnetic fields that are generated provide a means by which momentum and energy can be exchanged between the debris and air plasmas. However, in order to study this process it is important to first determine (1) the initial state of the target plasma and background gas (e.g., the state of ionization after the laser beam has been terminated) and (2) the influence of collisional processes on the interaction between the target and background species (e.g., charge exchange, ionization processes, electron stripping). The purpose of this report is to address several of these problems using existing NRL codes (i.e., UVDEP and PRODEP). Specifically, we study (1) the preionization of the background gas due to the initial radiation flash (UVDEP); (2) the energy degradation of the ions due to several collisional processes (e.g., elastic scattering, ionization, charge exchange) (PRODEP). (3) the ionization of the background gas due to the target ions (PRODEP); (4) and the ionization produced by uv from the interaction of debris ions with the background (UVDEP).

For all studies we use an aluminum target and a background N_2 gas. The laser energy is taken to be 100 joules, with 25 joules in prompt x-rays and a kinetic yield of the debris ions of 60 joules. We assume that there are 6.8×10^{10} aluminum ions released with average velocity of 6.7×10^{7}

Manuscript approved May 24, 1983.

cm/sec. The mass distribution of debris is assumed to obey a cosine law around the forward direction (Grun et al., 1983). All radiation is assumed to come from a point source.

The organization of the paper is as follows. In Section II we discuss the influence of prompt x-ray emission and deposition into the background nitrogen gas using the code UVDEP. In Section III we make use of the code PRODEP to study the energy degradation of the target ions due to several collisional processes, and the amount of background ionization produced by these ions. In Section IV we present a discussion of uv emission effects and in the final section offer some concluding remarks.

II. Prompt X-Ray Emission and Deposition

A. Discussion

In a HANE event x-rays are emitted during the disassembly process. The energy released from nuclear processes heats the materials of the structure to kilovolt temperatures. This results in the emission of blackbody thermal radiation from the core of the device which diffuses outward through the outer layers of the device and the surrounding rocket, reentry vehicle, etc., and radiates into the atmosphere. These prompt x-rays have long mean free paths in the upper atmosphere and deposit their energy out to distances of thousands of kilometers, or down to an altitude of $\sim$ 70 km. They ionize the atmosphere, altering it from its ambient state. It is this altered medium through which the bomb debris, the blast wave, the uv radiation, etc. subsequently must pass.

At NRL, a code has been developed, UVDEP, (Hyman, et al., 1971; Hyman, et al., 1977) which models the deposition both of prompt x-ray emission and the later uv emission, out to large distances from the burst. It tracks the resulting atmospheric chemistry in a time dependent way to times $\sim$ 1 sec, which in the HANE case is the time scale up to which hydrodynamic processes are not too important, the uv emission is essentially complete, and the 'fast' chemistry is completed. The chemistry includes a modeling of both molecular and atomic atoms and ions.

In the laser experiment it is necessary first to calculate the x-ray emission spectrum. The spectrum is not black body. The laser pulse causes ablation of the aluminum target forming an aluminum plasma. The pulse has a duration of several nanoseconds and the x-ray emission occurs over a time scale not much longer than this. Thus, as in the HANE case, the x-radiation is prompt compared to time scales for other phenomenology of interest. A detailed radiation-hydrodynamic model to simulate the x-ray emission induced by a laser pulse on an aluminum target has been constructed at NRL (Duston et al., 1983). Figure 1 illustrates schematically the various regions modeled in this simulation. The model determines the electron plasma temperature and the distribution of Aℓ charge states in each of the regions as a function of time. The x-ray emission is a result of bound-bound, bound-free, and free-free electron transitions of the various aluminum charge states present in the plasma at a given time. Thus, the spectrum calculated not only is not black body, but is also time dependent.

Different segments of the x-ray energy spectrum originate from different spatial regions. For example, more than three quarters of the energy for x-ray energies above ~ 1.5 kev is due to bound-bound transitions resulting from excitation of K-shell electrons of Aℓ XII and Aℓ XIII. These species occur in the hot blowoff region (Figure 1) where the electron plasma temperature is ~ 1 kev. Between ~ 0.5 kev and ~ 1.5 kev the x-ray spectrum is almost totally due to bound-free transitions, since this energy range corresponds to energies too small for K-shell transitions but too large for L-shell transitions. Below ~ 0.5 kev L-shell transitions from ions less ionized than Aℓ XII contribute substantially. These ions occur in the cooler transition region (Figure 1). In this energy region bound-free transitions represent the major contributor down to ~ 0.04 kev, with bound-bound still important down to ~ 0.1 kev. Below 40 ev free-free transitions predominate. Figure 2 shows the spectrum of the total x-ray energy emitted per square centimeter indicating separately the bound-free and free-free contributions as well as the bound-bound lines as predicted by the model. Figure 3 gives the energy spectrum of the intensity at a particular time, near the time of peak emission. The two are, not surprisingly, similar in overall shape but exhibit differences of detail. At other times, away from the time of peak emission, the differences may be

more pronounced. To approximate the x-ray spectrum for use in UVDEP we divided it into segments each of which is fit by a power law (straight line on a log-log plot). In performing this fit we were careful to maintain the model predictions of the fraction of photon energy in various photon bins (Table III, Duston et al., 1983).

We have considered the following cases: (1) N_2 density = 10^{14} cm^{-3}, scaled to a STARFISH density (400 km), (2) N_2 density = 10^{16} cm^{-3}, scaled to a standard SPARTAN density (200 km), and (3) N_2 density = 10^{17} cm^{-3}, scaled to CHECKMATE density (150 km). The scaling assumes that binary collisions in the HANE event and in the experiment play an equivalent role. However, when referring to these scaled HANE events one needs to keep in mind differences: the existence of an exponential atmosphere in the real event but not in the laser experiment; the fact that N_2 is not the only species in the real event, and not even an important one in the STARFISH case; and the fact that magnetic fields are not scaled properly in the experiment. Still, for the early time phenomenology, which is a primary goal for the experiment to simulate, these differences are either not crucial or can be accounted for, hopefully, by theory. Finally, in calculating the deposition of x-ray energy we have not accounted for the possible dependence of emission with angle in the forward direction. This is probably not a serious error, since the dependence should be weak except at very large angles.

B. Results

We first consider the case N_2 density = 10^{14} cm^{-3}, which corresponds to a scaled STARFISH altitude. Figure 4 is a plot of electron density as a function of distance from the target at three times subsequent to the passage of the x-rays. The first time, (1) t = 0 is the time just after the x-rays have been deposited but before any chemistry has occurred. The other two times are (2) t = 1 x 10^{-7} sec and (3) t = 5 x 10^{-6} sec after time t = 0. The upper scale gives an expanded picture of the first 10 cm and the lower shows the electron density dependence out to 70 cm.

Before continuing with a discussion of these results one important caveat needs to be stated. The following results concern only the effect of the x-rays. As the debris moves out, this is the environment it moves

into. Once the debris reaches a particular distance from the target, however, it will significantly change the electron density. Assuming the debris moves with a velocity of 6.7×10^7 cm/sec it will have reached out to 6.7 cm by 10^{-7} sec and, therefore, have altered the electron densities on this curve in Figure 4 closer in than 6.7 cm. By 5×10^{-6} sec, debris moving with 6.7×10^7 cm/sec will more than cover the entire region plotted in Figure 4. Generally speaking, where the debris has reached it will have caused much more ionization than the x-rays (see Section III). Because the debris mass tends to be peaked in the forward direction with a dependence $\sim \cos \theta$, θ the angle away from forward, off-angle its effect is likely to be less dominant over the x-ray effect than is the case in the forward direction.

More important is the question of whether the debris will continue moving out with this velocity indefinitely or will couple with the background and lose its kinetic energy. If it couples, its directed energy will likely be significantly altered once it interacts with a weapon mass of background. If the background were fully ionized, this corresponds to a weapon radius of a few centimeters for this density (see section III). However, the average ionization in this region due to x-rays is only $\sim$ 10%, so that a true weapon mass corresponds to a much larger dimension, unless there is a mechanism for coupling with the neutral atmosphere or via an anomalous ionization process. If coupling does occur the beam will be slowed or stopped and the results in Figure 4 will be valid beyond that radius. When the debris interacts with the N_2 it will generate hot electrons with a temperature and for a duration that depends on the nature of the coupling, collisional or non-collisional. The hot electrons will excite electronic levels in the debris-air mixture resulting in uv emission. The uv will be deposited mostly outside the debris-coupling region, but on the average at closer distances than the x-rays and will, in general, greatly alter the electron densities outside the coupling region. In the example being discussed here, N_2 density = 10^{14} cm^{-3}, we do not expect uv emission to be important, whether coupling occurs or not, just as it was not important in STARFISH. Uv effects will be described in Section IV.

With the above provisos, let us take a more careful look at the x-ray results. After the initial ionization of N_2 by the x-rays we are left with hot electrons throughout the mesh (20-30 ev). These electrons further ionize N_2, at first, and also begin dissociatively recombining the N_2^+. The resulting N and $N(^2D)$ can also be ionized by the still hot electrons. Thus, the initial effect of the chemistry is to increase the electron density. Because of the high N_2 density, the electrons cool predominantly by ionizing N_2, so that the electron temperature at a given time is nearly independent of distance from the target, except very near the target where N_2 has been depleted. Figure 5 shows the time dependence of the electron density and temperature at three distances from the target: (1) 0.5 cm, (2) 5.0 cm, and (3) 50. cm. The temperature curves are nearly identical at 5.0 cm and 50. cm. At 0.5 cm, where the N_2 has been depleted, the temperature is essentially constant by 2×10^{-6} sec. The electron density here has already begun to drop by a few times 10^{-7} sec because of the depletion of neutrals even though the electron temperature is still high. At greater distances, where depletion of neutrals has not occurred and when the electron temperature has cooled to ~ 2 ev, ionization is no longer important and the electron density begins to decrease. Figure 6 shows the densities of N_2, N_2^+, N^+, N, and $N(^2D)$ and the electron temperature (T_e) as a function of distance from the target at 10^{-7} sec. The near constancy of electron temperature with distance from the target, discussed above, can be seen here. We see that N_2^+ is everywhere the major ion constituent. As electron temperatures drop or neutral species are depleted, electron densities stop increasing. But the time scales to deplete electrons are longer than the time scales exhibited here. N_2^+ dissociatively recombines with a rate coefficient between 10^{-7} cm^3/sec - 10^{-8} cm^3/sec at these temperatures, which gives a time scale for depletion of electrons, even where $N_2^+ \sim 10^{13}$ cm^{-3}, of 10^{-6} - 10^{-5} sec. This is also, of course, the time scale for the buildup of N and $N(^2D)$. N^+ recombines radiatively on a much slower time scale. Thus, except for the electron temperature, which drops fairly rapidly (Figure 5), the profiles shown in Figure 6 will not change in time significantly until (and unless) the debris or uv alters the state of affairs.

We next consider the case N_2 density = 10^{16} cm^{-3} which scales to a "standard altitude" SPARTAN. Here uv emission is likely to be important, but we will postpone the analysis of uv effects to Section IV and consider only the effects of x-rays. For the laser experiment at this density, if the background is totally ionized, a weapon radius is $\lesssim$ 1 cm. Figure 7 shows electron densities as a function of distance from the target, due to x-ray deposition, for several times after deposition. These curves suggest that the debris probably does intercept a weapon mass within a few centimeters of the target. The times plotted are (1) t = 0.0, (2) 1 x 10^{-8}, (3) 1 x 10^{-7}, and (4) 5 x 10^{-7} sec after deposition. If coupling does not occur, only the nearest 0.67 cm would be altered for the t = 10^{-8} sec curve. At 10^{-7} sec, 6.7 cm would be changed by the debris, and at 5 x 10^{-7} sec the entire plotted curve would be altered. If coupling does occur, the beam would probably be stopped in the first few centimeters, but uv emission and deposition would then alter the x-ray results. Neglecting these effects, for the moment, we now consider the x-ray only results in more detail.

In contrast to the N_2 density = 10^{14} cm^{-3} case, processes with the N_2 density = 10^{16} cm^{-3} occur much faster. At 1.0 cm the electron density appears in Figure 7 to drop monotonically from the time zero value to its value at t = 5 x 10^{-7} sec. What, in fact, has happened is the electron density has peaked by t $\sim$ 3 x 10^{-9} sec. The major ion at this time is N_2^+, which from then on decreases at a faster rate than new ions are produced, since the electron temperature is dropping very rapidly. By t = 1 x 10^{-7} sec, at 1.0 cm, the N_2^+ has been substantially depleted (Figure 8), N^+ is the major ion and the major neutral constituents are N and N(^{2}D). At later times the N_2^+ continues to deplete, building up N and N(^{2}D) somewhat more, but N^+ remains virtually unchanged because of the long time constant for radiative recombination of N^+ and the low electron temperature, which excludes substantial ionization.

At larger distances, the time scales are, of course, somewhat slower. At 10 cm, at time t = 10^{-7} sec, N_2^+ is still the major constituent at $\sim$ 2.5 x 10^{13} cm^{-3}. The temperature is very low, cutting off ionization. The N_2^+ will continue to drop until by several times 10^{-6} sec it will be

below the N^+ value. From then on the electron density will remain essentially constant at a value $n_e \sim 1.5 \times 10^{12}$ cm^{-3} for a long time.

Finally, we plot the N_2 density = 10^{17} cm^{-3} case, scaled to a CHECKMATE altitude. A weapon mass of ionized background N_2 will be intercepted within about 0.5 cm of the target. Assuming coupling occurs, uv emission and deposition will be very important in altering the electron densities derived from x-ray deposition. Figure 9 is a plot of the x-ray induced electron densities at times (1) t = 0.0, (2) 5×10^{-9}, (3) 1×10^{-8}, and (4) 2×10^{-7} sec. The general characteristics are similar to the N_2 density = 10^{16} cm^{-3} case. Very close in (less than 0.4 cm) the temperature is high enough, and the N_2^+ has been recombined, so that electron densities are increasing. Slightly further out, (say, 0.4-0.7 cm) the temperature is too low for ionization to increase the electron density, but the N_2^+ density is small compared to N^+ so that the electron density is not changing, and the different curves in Figure 9 are merged. Beyond this region, N_2^+ is important, and its recombination governs the decrease in electron density and increase in N and $N(^2D)$. Ionization is not important because of the low electron temperature. Figure 10 shows the individual species and the electron temperature at t = 1×10^{-8} sec.

III. Ion Energy Degradation and Background Ionization

A. Discussion

We study the energy degradation of the ion beam due to several collisional processes, and the amount of background ionization produced by the beam using the code PRODEP. PRODEP is a code which was developed at NRL to study proton deposition in the atmosphere (Rogerson and Davis, 1974; Rogerson and Davis, 1975). The code is one-dimensional and is based upon the continuous slowing down approximation (CSDA). The collisional effects included in PRODEP are collisional ionization, electron stripping, charge exchange, and elastic collisions. PRODEP does not account for any interactions between the debris and background ions. We have modified PRODEP to study the case of a beam of aluminum ions ($A\ell^+$) propagating through a nitrogen gas (N_2). We consider a set of parameters relevant to

the NRL laser experiment and present results pertaining to (1) the energy degradation of the aluminum ion beam due to collisional effects, and (2) the ionization of the nitrogen gas due to the ion beam.

The fundamental equation used in the CSDA is

$$dE = - F(x)\ L(E)\ dx \qquad (1)$$

where dE is the incremental energy change in the ion beam in kev as it traverses a distance dx through a background gas of F(x) atoms per cm^2. In Eq. (1), L(E) is the ion energy loss function in kev cm^2/atom and is comprised of four parts in our model. Specifically,

$$L(E) = \text{ionization} + \text{electron stripping} + \text{charge exchange} + \text{elastic collisions} \qquad (2)$$

The reactions considered are

1. Ionization

$$Al + N_2 \rightarrow Al + N_2^+ + e$$

$$Al^+ + N_2 \rightarrow Al^+ + N_2^+ + e$$

2. Electron stripping

$$Al + N_2 \rightarrow Al^+ + N_2^* + e$$

3. Charge exchange

$$Al^+ + N_2 \rightarrow Al + N_2^+$$

The cross sections for these reactions were provided by Rogerson (private communication). Further details of the code can be found in Rogerson and Davis (1974) and Rogerson and Davis (1975).

Prior to discussing the results from PRODEP for the NRL laser experiment it is important to note the assumptions used in the code. First, it is assumed that the fractional energy loss per process is small. Second, the code is one-dimensional so that the scattering process is assumed to be symmetric. Third, only singly ionized states are considered. And fourth, it is assumed that the ions interact only with a neutral background gas. We point out that not all of these assumptions are well-justified in the NRL experiment. In particular, (1) the debris ions do not come off the target in a spherically symmetric manner; (2) there are indications that the debris ions are in multiple charge states that vary in time (J. Grun, private communication); and (3) close to the target the assumption of a predominately neutral gas clearly breaks down. Thus, the results from PRODEP must be interpreted with care in attempting to relate them to the NRL experiment. Nonetheless, several of the results are pertinent to the experiment and provide a good, first-order understanding of some of the collisional processes occurring in the experiment.

B. Results

We now present PRODEP results for conditions relevant to the NRL experiment. It is implicitly assumed that coupling has not occurred. An important quantity used in the analysis is F which is the number of molecules encountered per cm^2. In order to make contact with experimental results, the following relationship is used

$$F = n\ell \tag{2}$$

where n is the density of the background gas (cm^{-3}) and ℓ is the distance the ions have travelled in the background gas (cm). Thus, for a given F used in the code, different values of n and ℓ can be applied to the experiment through Eq. (2).

The initial energy distribution for the ion beam ($A\ell^+$) is given by

$$\Gamma(E) = \frac{\Delta E^2}{(E-E_o)^2 + \Delta E^2} \tag{3}$$

where E_o = 60 kev, $\Delta E = 0.23E_o$. The total energy in the ion beam is 60 joules. The average initial ion velocity of the beam is $V_o = 6.7 \times 10^7$ cm/sec with an energy flux of 4.8×10^{15} kev/cm^2. This value of the flux

corresponds to an average flux at 3.5 cm from the target, or to the flux at 4.2 cm in the forward direction in the laser experiment.

We first present "time of flight" curves (Figure 11) and the energy distribution (Figure 12) corresponding to each curve. The "time of flight" curves are shown since they correspond to the type of measurements made in the NRL experiment (J. Grun, private communication). To facilitate comparison with the experiment, and to make the results depend only on F, the time is normalized so that an ion of average energy E_o in vacuum will impact the detector at $t_{norm} = 70$ on a scale 0 to 256 (i.e., $t_{norm} = 70\ V_o t_{real}/\ell$). In Figure 11 we show "time of flight" curves for the initial conditions described above and taking $F = 10^{15}$, 10^{16}, 10^{17}, 5×10^{17} and 10^{18} cm^{-2}. The plot is number of particles on an arbitrary scale versus normalized time. The curves for $F = 10^{15}$ and 10^{16} cm^{-2} are indistinguishable and are effectively the same as would arise if $F = 0$ (i.e., an ion beam propagating through a vacuum). The ions to the left of the peak (at $t \sim 70$) are the "fast" particles ($E > 60$ kev) while those to the right of the peak are the "slow" particles ($E < 60$ kev). Note that the "time of flight" curves are not symmetrical about the peak, while the energy distributions (Figure 12) are symmetrical. Thus, for $F \leq 10^{16}$ cm^{-2} we see that there is no energy degradation of the ion beam because of collisional interactions with the background gas. For $F = 10^{17}$ cm^{-2} (or $n = 10^{16}$ cm^{-3} for $\ell = 10$ cm) the "time of flight" curve is slightly displaced from the $F = 10^{16}$ cm^{-2} curve (Figure 11), while there is a more noticeable change in the energy distribution (Figure 12). As F increases further, $F = 5 \times 10^{17}$ and 10^{18} cm^{-2} (or $n = 5 \times 10^{16}$ or 10^{17} cm^{-3} for $\ell = 10$ cm), a significant change in the "time of flight" curves (Figure 11) occurs, along with a marked change in the energy distribution. The peak of the "time of flight" curves shift to the right, indicating a slowing down of the "average" velocity of the beam, and the curves become broader. However, the broadening of the "time of flight" curves does not correspond to a broadening of the energy distribution. Note that the energy distributions for $F = 5 \times 10^{17}$ and 10^{18} cm^{-2} (Figure 12) maintain approximately the same width ΔE but the peak energy E_o decreases significantly. We expect that in the experiment the ion beam (i.e., debris ions) will broaden its energy distribution if energy degradation occurs.

PRODEP does not entirely account for this effect because in each energy channel all ions are slowed by the same amount, with no allowance for statistical variations.

The results shown in Figs. 11 and 12 are consistent with measurements made to date in the NRL laser experiment, although a detailed comparison cannot be made at this time. The reason for this is that the existing PRODEP code can only treat an aluminum target and nitrogen background, while the relevant existing data from the experiment is for a carbon target with nitrogen and hydrogen backgrounds. Nonetheless the experimental results presented by J. Grun at the DNA NRL meeting in January, 1983 indicated that for $F \lesssim 4 \times 10^{16}$ cm^{-2} the debris "time of flight" curves were essentially unchanged from the vacuum case. This agrees with our results shown in Fig. 11 which indicate that for $F \lesssim 10^{17}$ cm^{-2} the "time of flight" curves are virtually the same. Clearly, a more detailed comparison is needed to assess the predictions made by PRODEP in regard to the NRL laser experiment.

In Figure 13 we show a plot of percent of background primary ionized gas (N_2^+/N_2) as a function of distance for the average flux. Three curves are shown, $n = 10^{14}$, 10^{16} and 10^{17} cm^{-3}. For the most part $N_2^+/N_2 \propto 1/r^2$ in each case but, as expected, there is more absorption of the beam at the higher n values. These curves are only correct for $x \gtrsim 3.5$ cm at which $N_2^+/N_2 \simeq 9\%$. If we extrapolate these curves to the regime $x \lesssim 3.5$ cm as denoted by the dotted line, they will intersect 100% ionization near 1. cm. The dashed curves show the percent of primary ionization produced by x-rays for these same densities. For both the x-rays and the beam the $F = 10^{14}$ curves fall off as $1/r^2$ but at the larger densities absorption causes the curves to fall off faster. For all densities the ionization produced by the ions is about an order of magnitude greater than that produced by the x-rays. Directly in front of the target the 9% ionization distance occurs at 4.2 cm so the difference is even greater. The results presented here are primary ionization with no effects of chemistry. The electron density and ion composition will change in time due to chemistry effects in a manner similar to that described in Section II.

IV. Uv Emission Effects

Until we have completed development of our early time codes which specify when coupling occurs, the nature of the coupling, and the resulting uv emission, we cannot predict with certainty whether the debris will be slowed, and if so, how far from the target, and what portion of the beam kinetic yield will be converted to uv. Consider, first, the N_2 density = 10^{16} cm^{-3} case. In the laser experiment approximately 60% of the yield is kinetic so that uv effects are potentially more important than would be the case in a typical HANE event. To bracket the likely effects of uv we have considered two possible cases: (1) uv yield 30% of kinetic and (2) uv yield 60% of kinetic. In discussing these results one must understand that they are based upon debris-background coupling. The debris loses its energy so that it does not continue moving out from the target much past a few cm, and has a substantial portion of its directed energy converted to uv radiation. The code UVDEP assumes the uv originates from a point source at the target, an assumption that is not terribly good near the target. We have used a uv spectrum obtained from CHECKMATE calculations, which is a relatively low energy uv spectrum. The hardness of the spectrum, which can only be determined from full early time calculations may also affect the results given here.

Figure 14 shows the electron density as a function of distance from the target at $t = 5 \times 10^{-7}$ sec with no uv and at $t = 5.5 \times 10^{-7}$ sec for the two cases, 30% and 60% of the kinetic yield in uv. Clearly, the uv very significantly alters the ionization. The time dependence of the electron density for two points distant 2 cm and 10 cm, respectively, from the target is exhibited in Figure 15. The uv is emitted in time with 57% emitted by $t = 2 \times 10^{-7}$ sec and 98% by $t = 5.5 \times 10^{-7}$ sec. Consequently, at each point the electron density for the different cases initially begins falling in the same way. As the uv deposition builds up, the curves diverge with the electron density increasing. Only after the bulk of the uv has been emitted does the electron density begin to fall again. The effect of uv is clearly significant under the assumptions we have made.

Consider, now the N_2 density = 10^{17} cm^{-3} case. At this higher density we expect a higher uv yield than in the previous example. We consider two cases here: (1) 62% of the kinetic yield is converted to uv radiation and

(2) 90% of the kinetic yield is converted to uv radiation. If coupling occurs the debris should be stopped within ~ 1 cm. Figure 16 shows the electron density profile for no uv at $t = 1 \times 10^{-7}$ sec and for 62% and 90% of the kinetic yield converted to uv at $t = 1.1 \times 10^{-7}$ sec. The interesting point here is that at a density of 10^{17} cm^{-3} the uv is essentially totally absorbed within a distance of ~ 5 cm. from the target. At closer in distances the uv is clearly important. At 2 cm from the target the uv has increased the electron density by more than an order of magnitude at 10^{-7} sec.

V. Concluding Remarks

We have made a preliminary investigation of the role of radiation and collisional effects in the NRL laser/HANE experiment. The issues we have addressed are (1) the preionization of the background gas due to the initial radiation flash; (2) the energy degradation of the ions due to the several collisional processes (see Eq. (2)); (3) the ionization of the background gas due to the target ions; and (4) the ionization produced by uv radiation from the interaction of debris ions with the background gas. Our study has been based upon existing NRL codes (UVDEP and PRODEP) and considers an aluminum target and a background nitrogen gas. We have also considered parameter regimes accessible to the NRL experiment which scale (via binary collisions) to STARFISH, SPARTAN and CHECKMATE events. We emphasize that certain assumptions made in the codes are uncertain and/or violated to some extent within the context of the experiment since they were developed for actual HANE phenomena. Hence, the results must be considered preliminary and first order. More viable results depend upon further developments in early-time modeling currently underway at NRL.

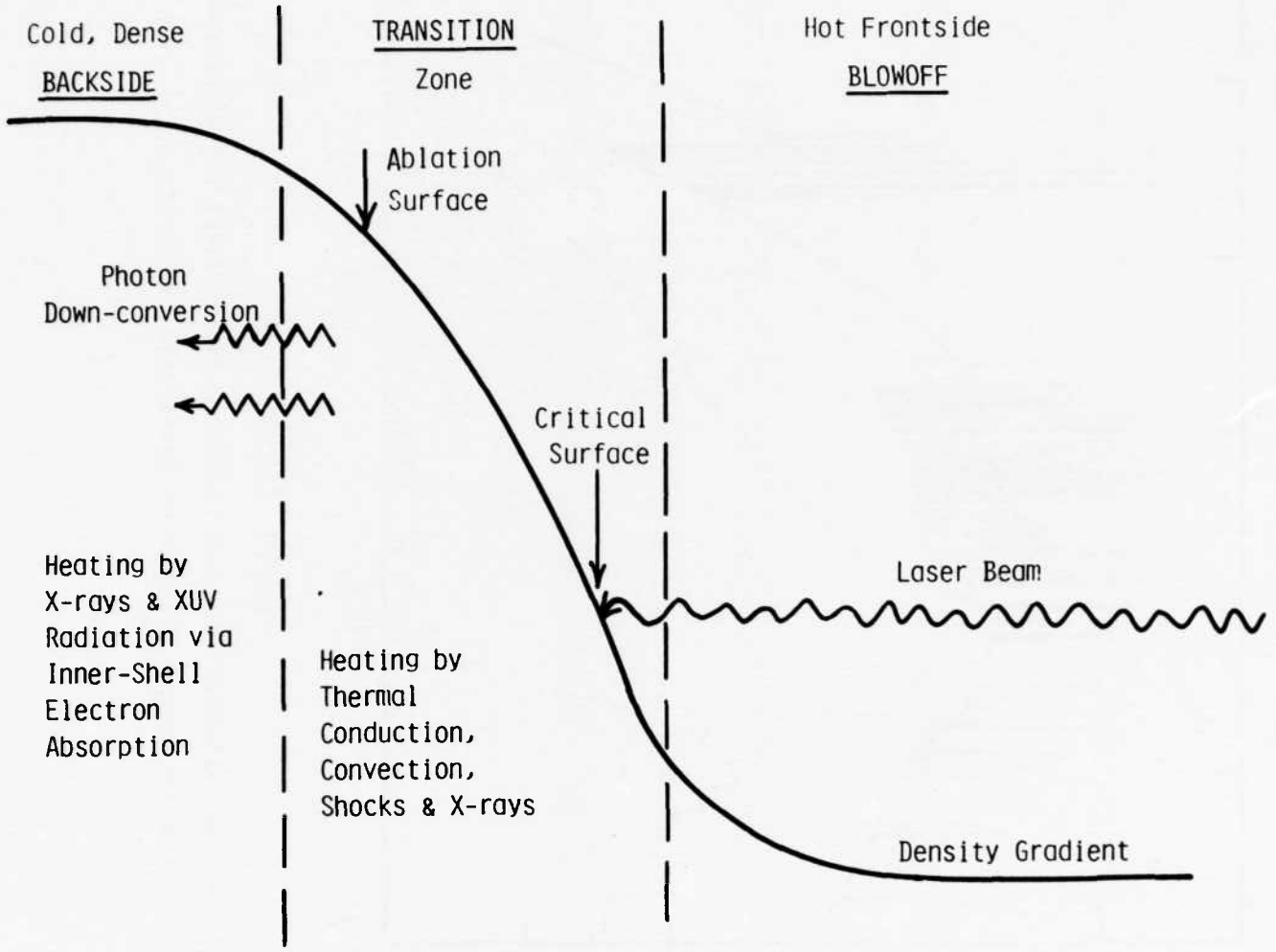

Figure 1 Laser-target simulation regions.

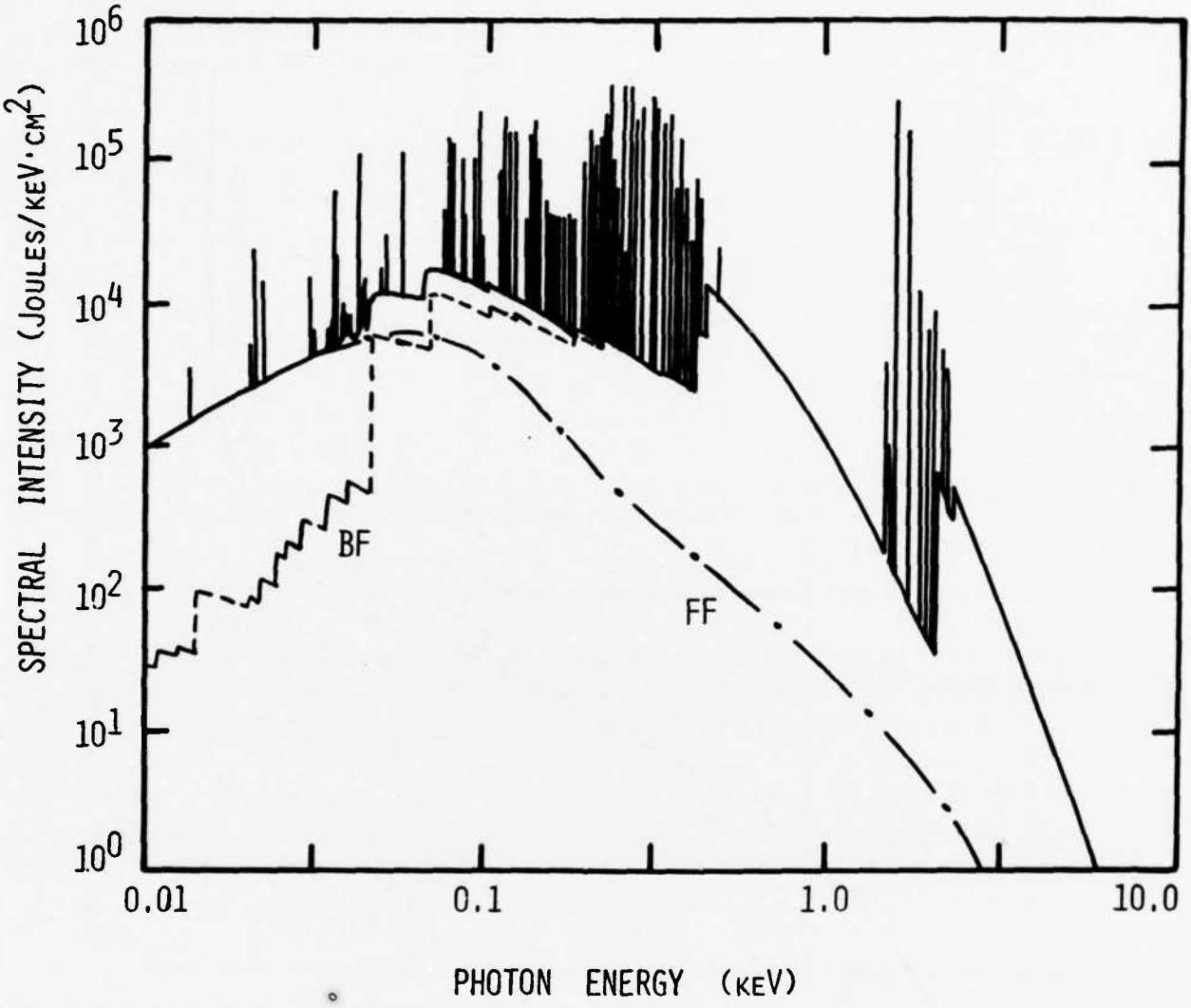

Figure 2 X-ray spectrum of total energy emitted by laser irradiated aluminum target per square centimeter of target.

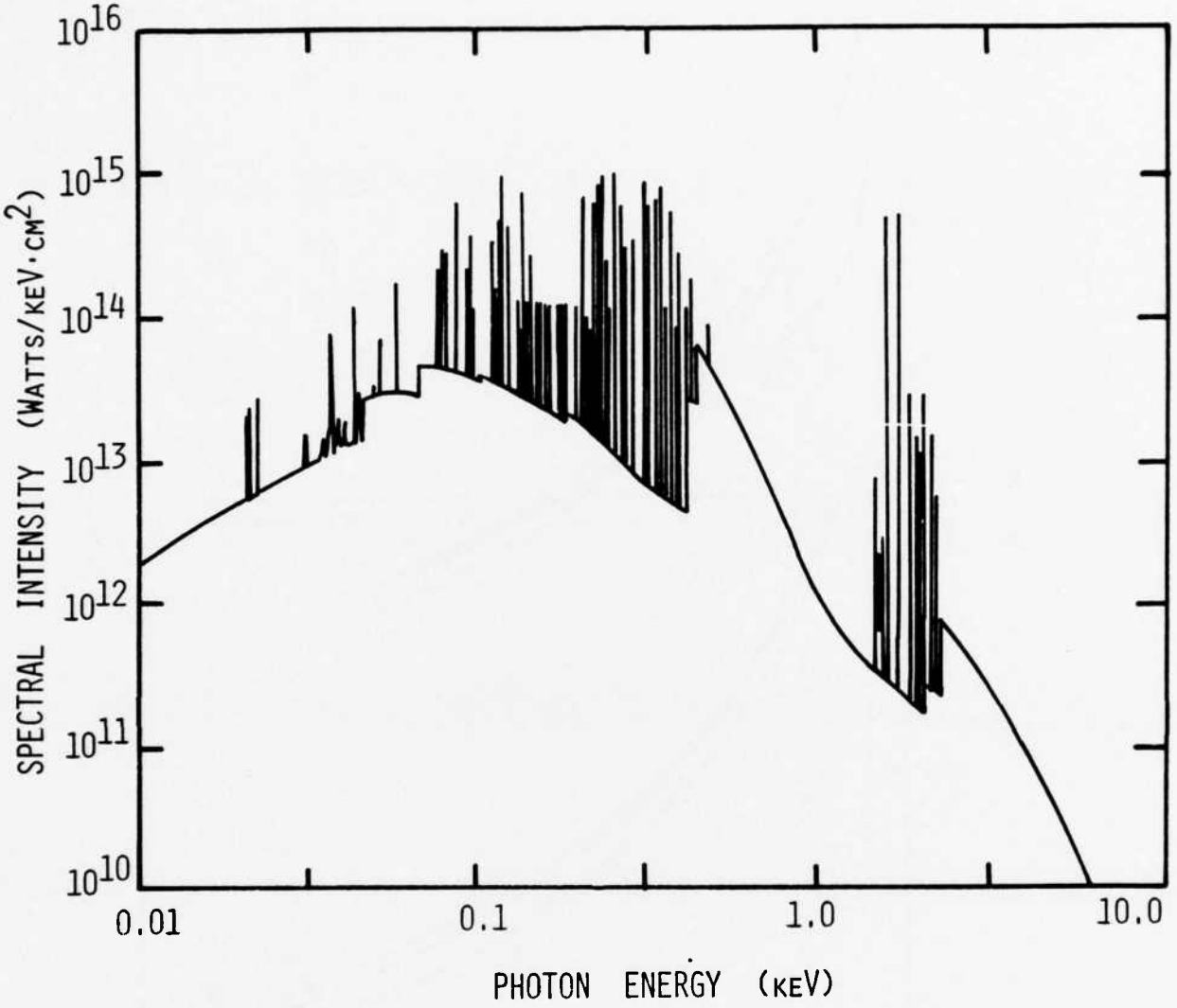

Figure 3 X-ray spectral intensity near time of peak emission of laser irradiated aluminum target.

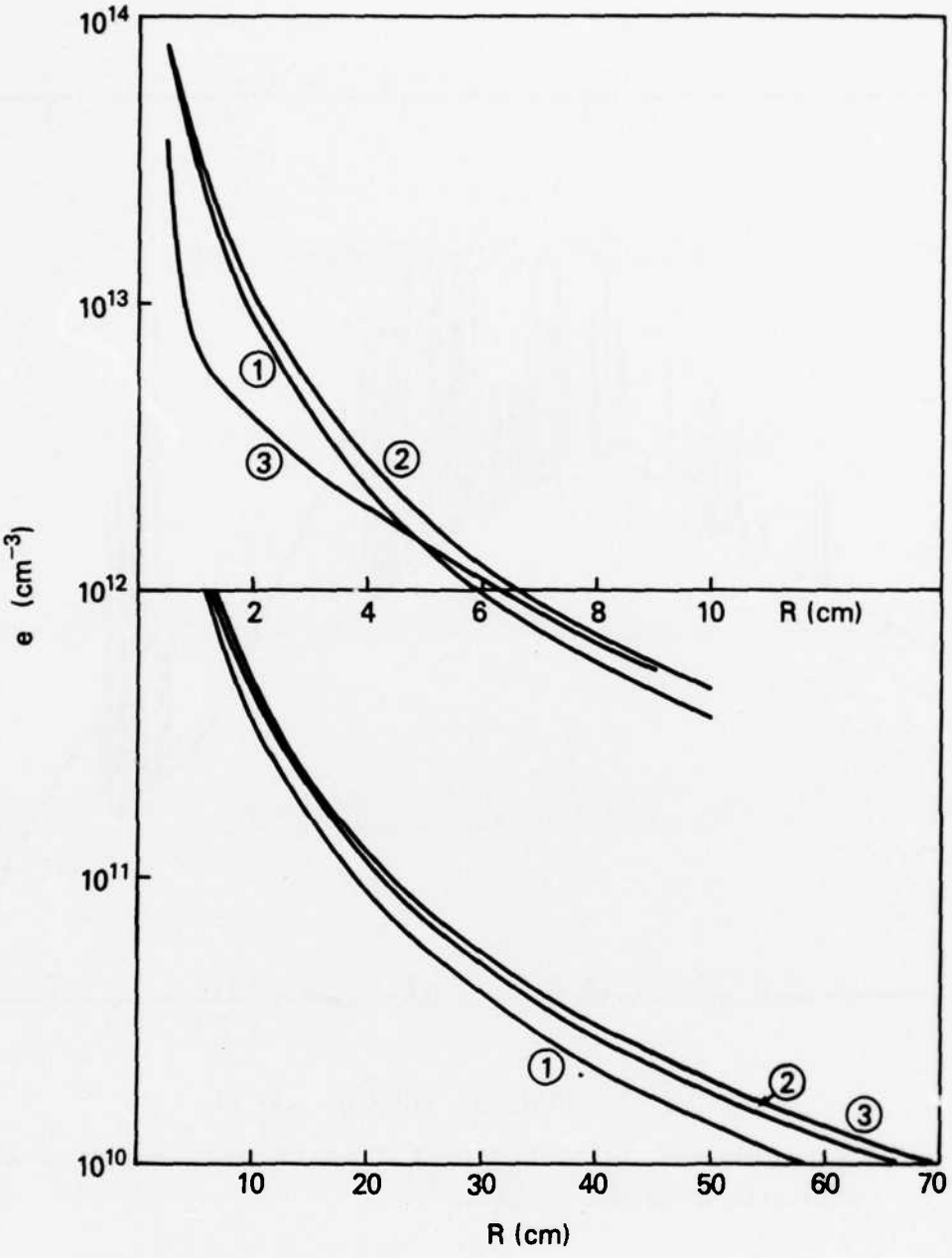

Figure 4 Electron density as a function of distance from target: (a) Upper scale = first 10 cm, (b) Lower scale = to 70 cm. Ambient N_2 = 10^{14} cm^{-3}. Curve labels give time after x-ray deposition: (1) = 0.0 sec, (2) = 1 x 10^{-7} sec, (3) = 5 x 10^{-6} sec.

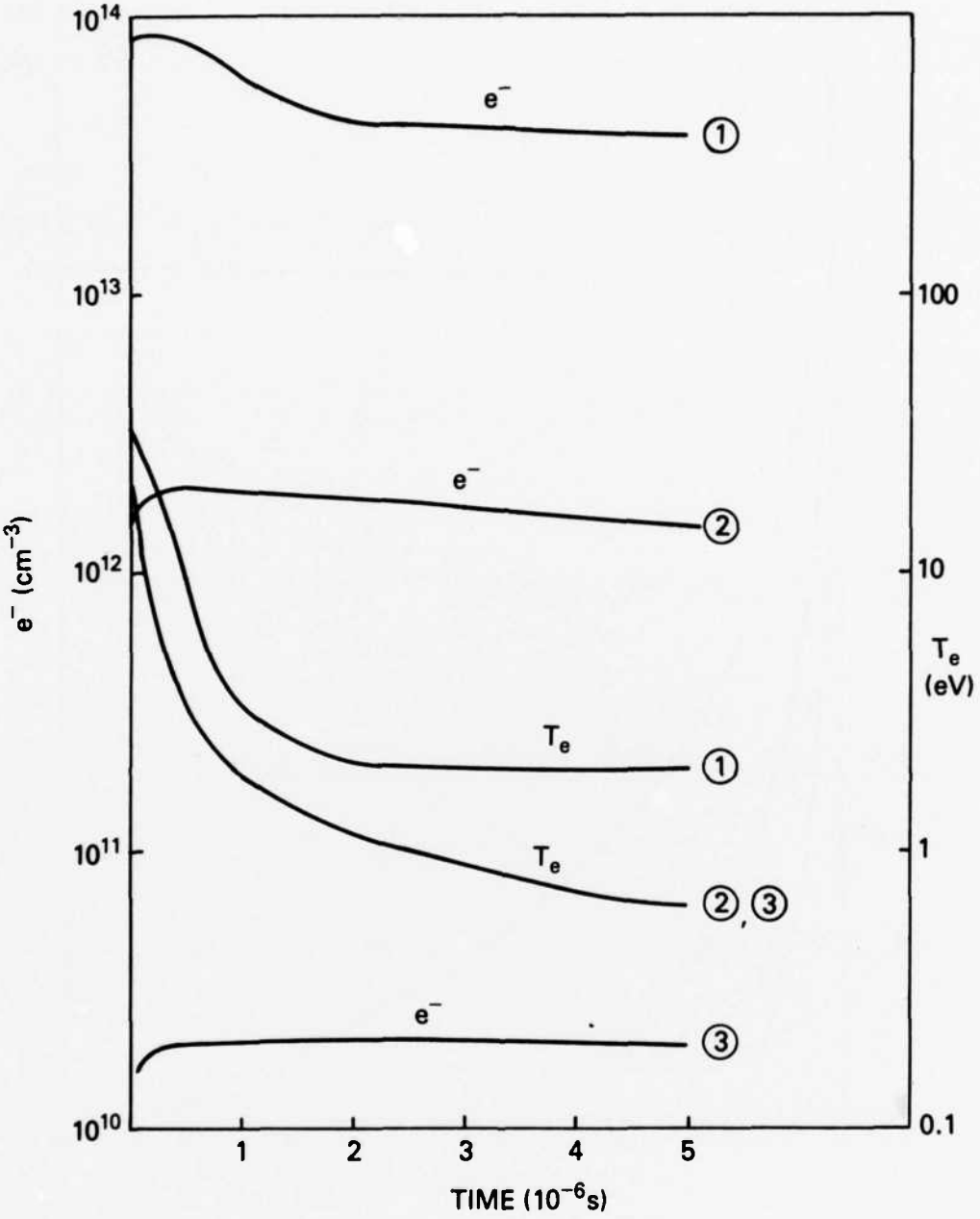

Figure 5 Electron density and temperature as a function of time after x-ray deposition at three distances from target: (1) 0.5 cm, (2) 5.0 cm, and (3) 50. cm. Ambient $N_2 = 10^{14}$ cm^{-3}.

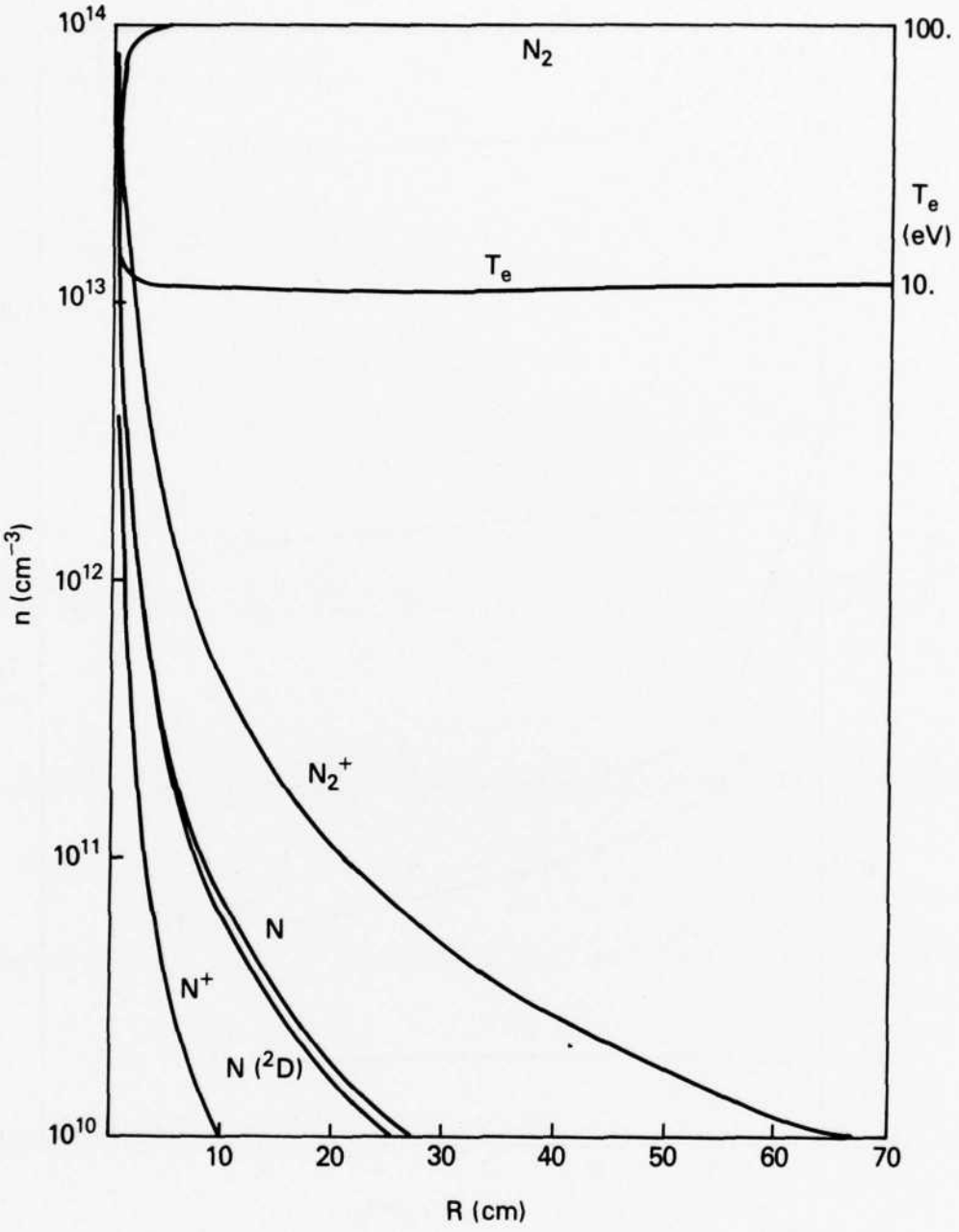

Figure 6 Specie densities and electron temperature at 1 x 10^{-7} sec after x-ray deposition as a function of distance from the target. Ambient N_2 = 10^{14} cm^{-3}.

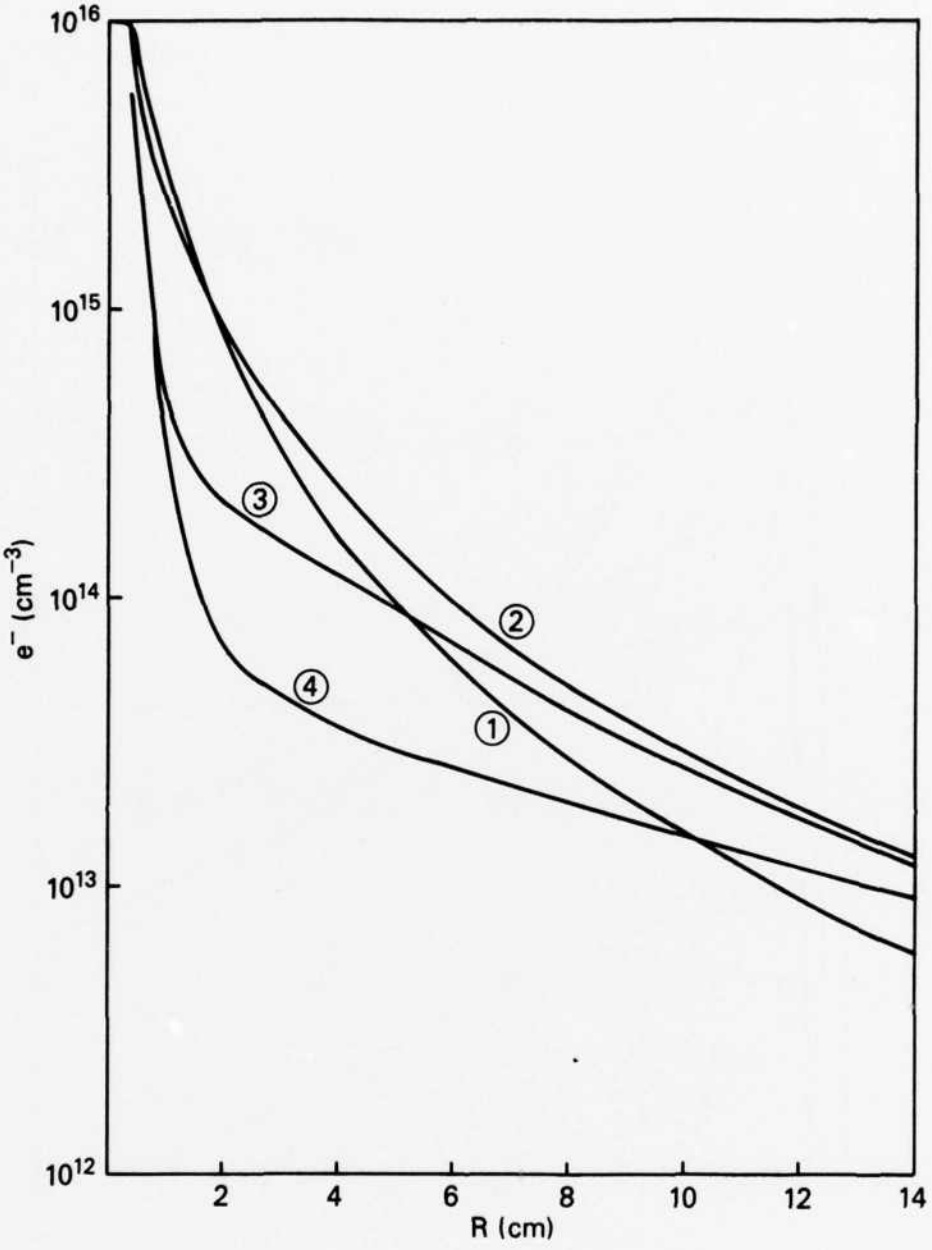

Figure 7 Electron density as a function of distance from target. Ambient N_2 = 10^{16} cm^{-3}. Curve labels give time after x-ray deposition: (1) = 0.0 sec, (2) 1 x 10^{-8} sec, (3) = 1 x 10^{-7} sec, (4) = 5 x 10^{-7} sec.

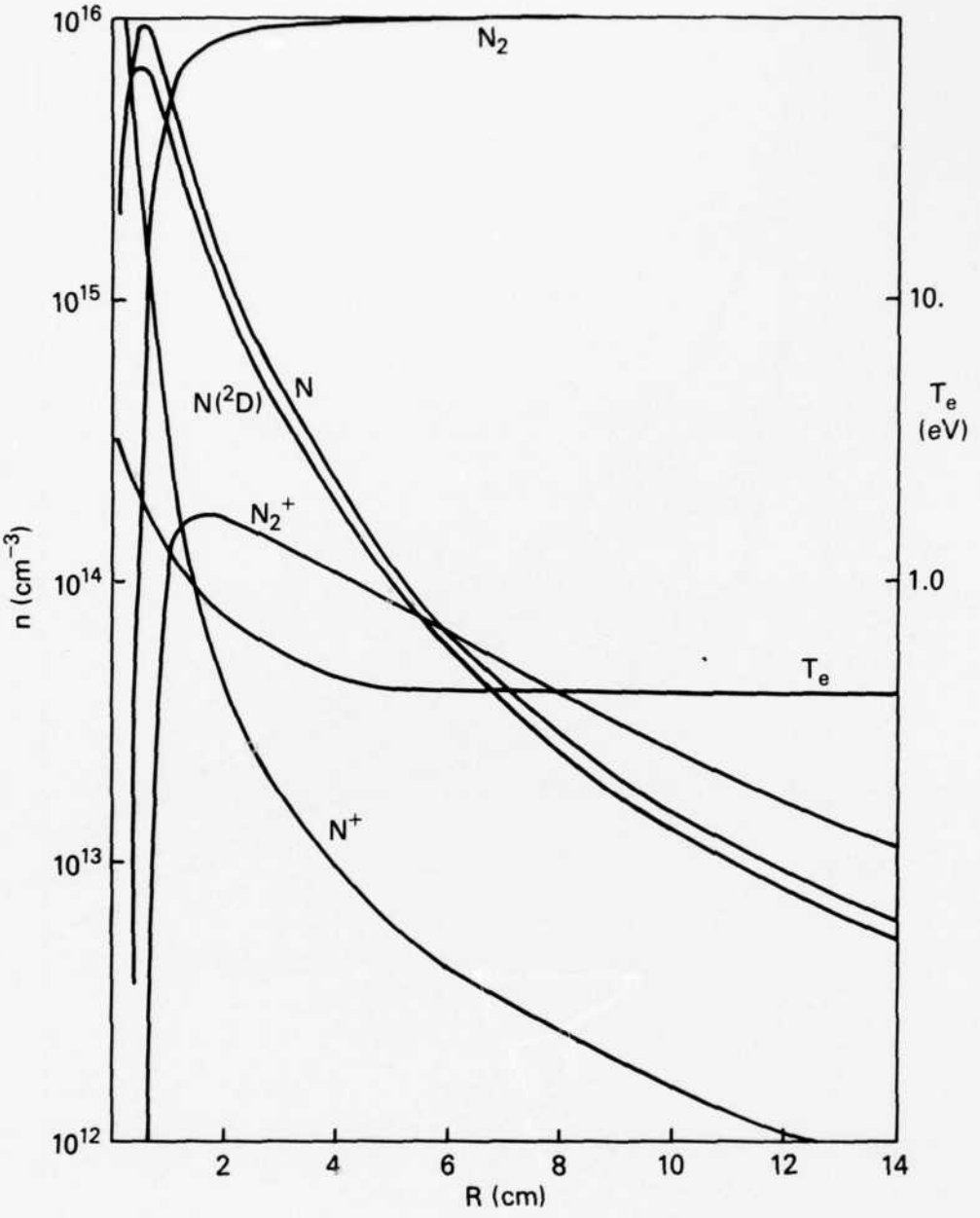

Figure 8 Specie densities and electron temperature at 1 x 10^{-7} sec after x-ray deposition as a function of distance from the target. Ambient N_2 = 10^{16} cm^{-3}.

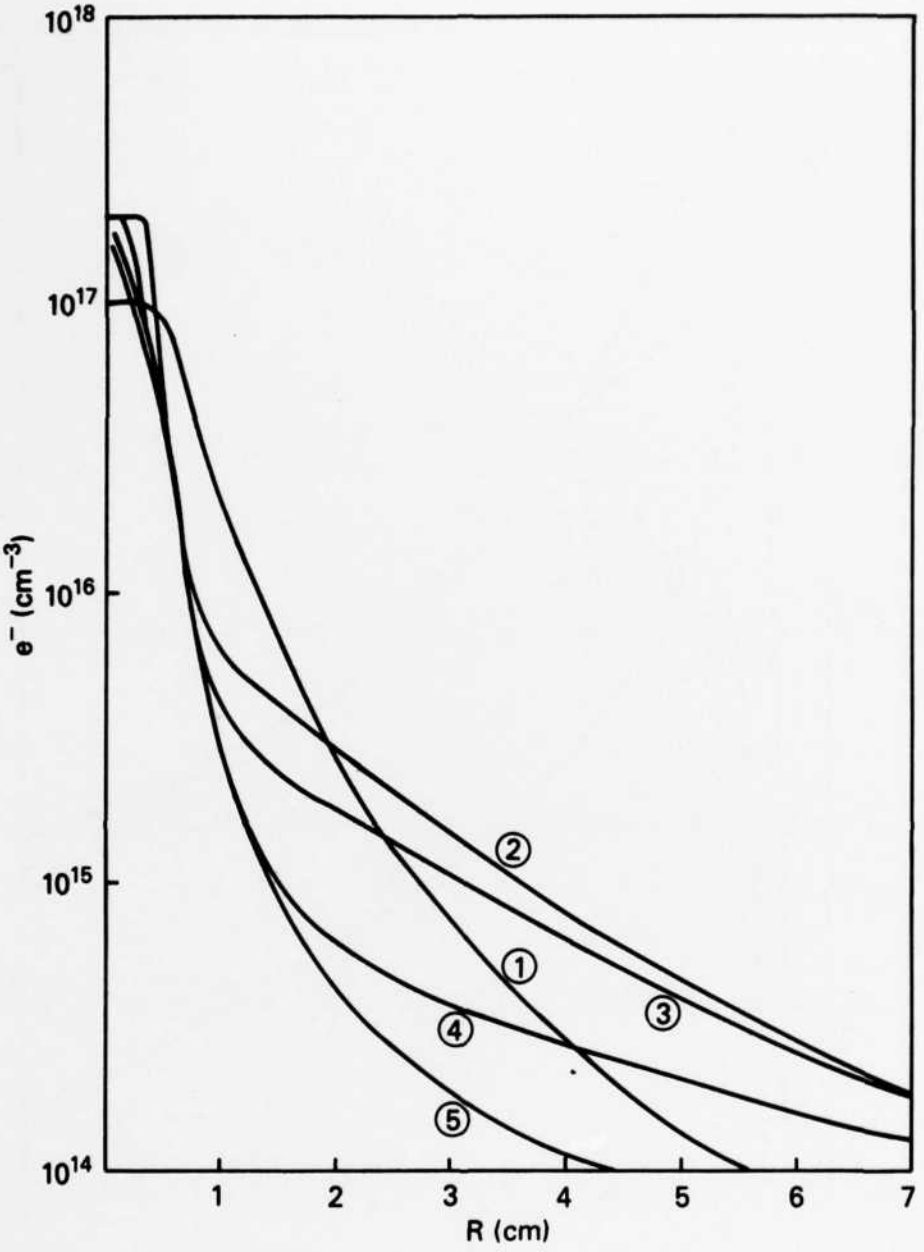

Figure 9 Electron density as a function of distance from target. Ambient N_2 = 10^{17} cm^{-3}. Curve labels give time after x-ray deposition: (1) = 0.0 sec, (2) = 5 x 10^{-9} sec, (3) 1 x 10^{-8} sec, (4) 5 x 10^{-8} sec, (5) = 2 x 10^{-7} sec.

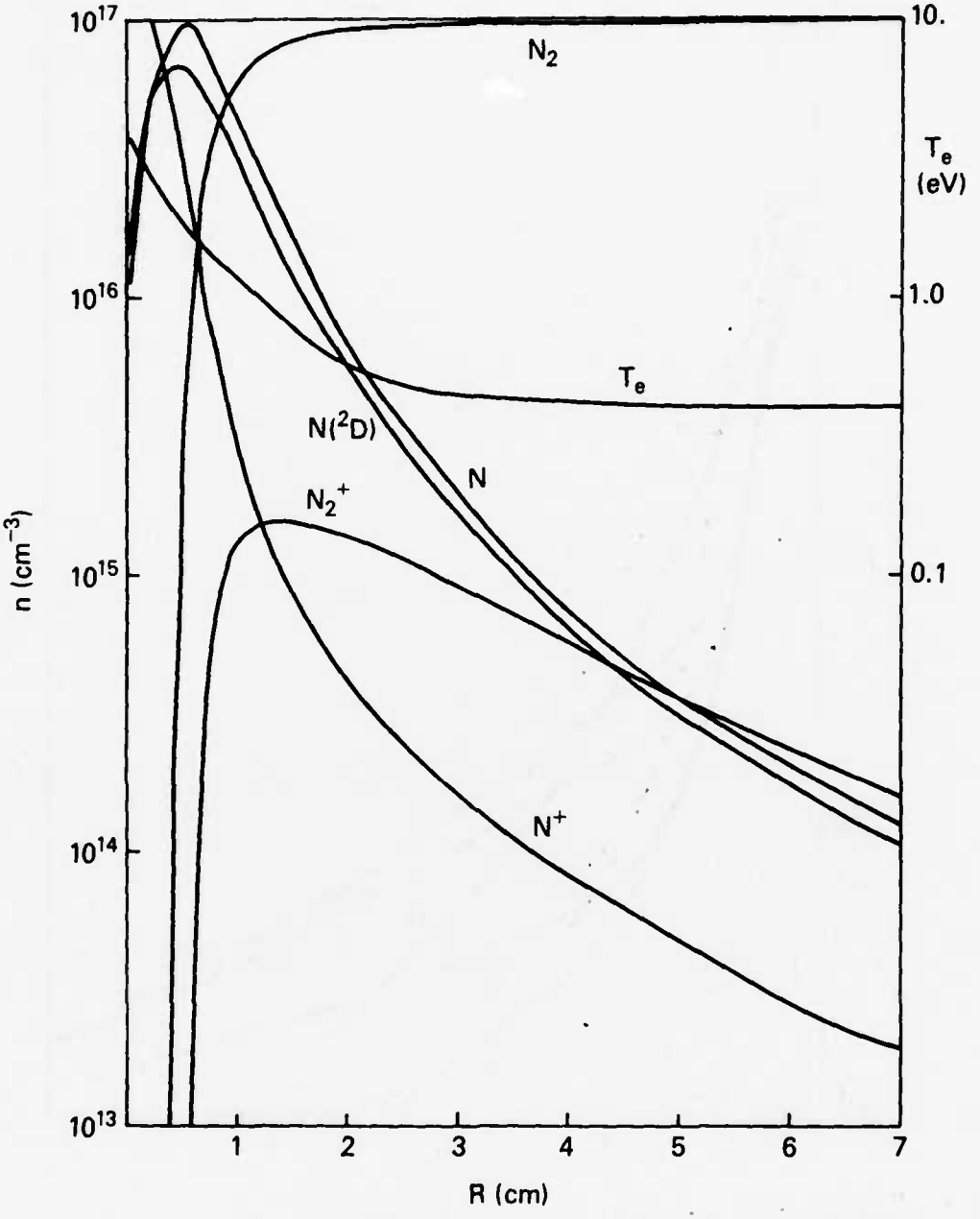

Figure 10 Specie densities and electron temperature at 1×10^{-8} sec after x-ray deposition as a function of distance from the target. Ambient $N_2 = 10^{17}$ cm^{-3}.

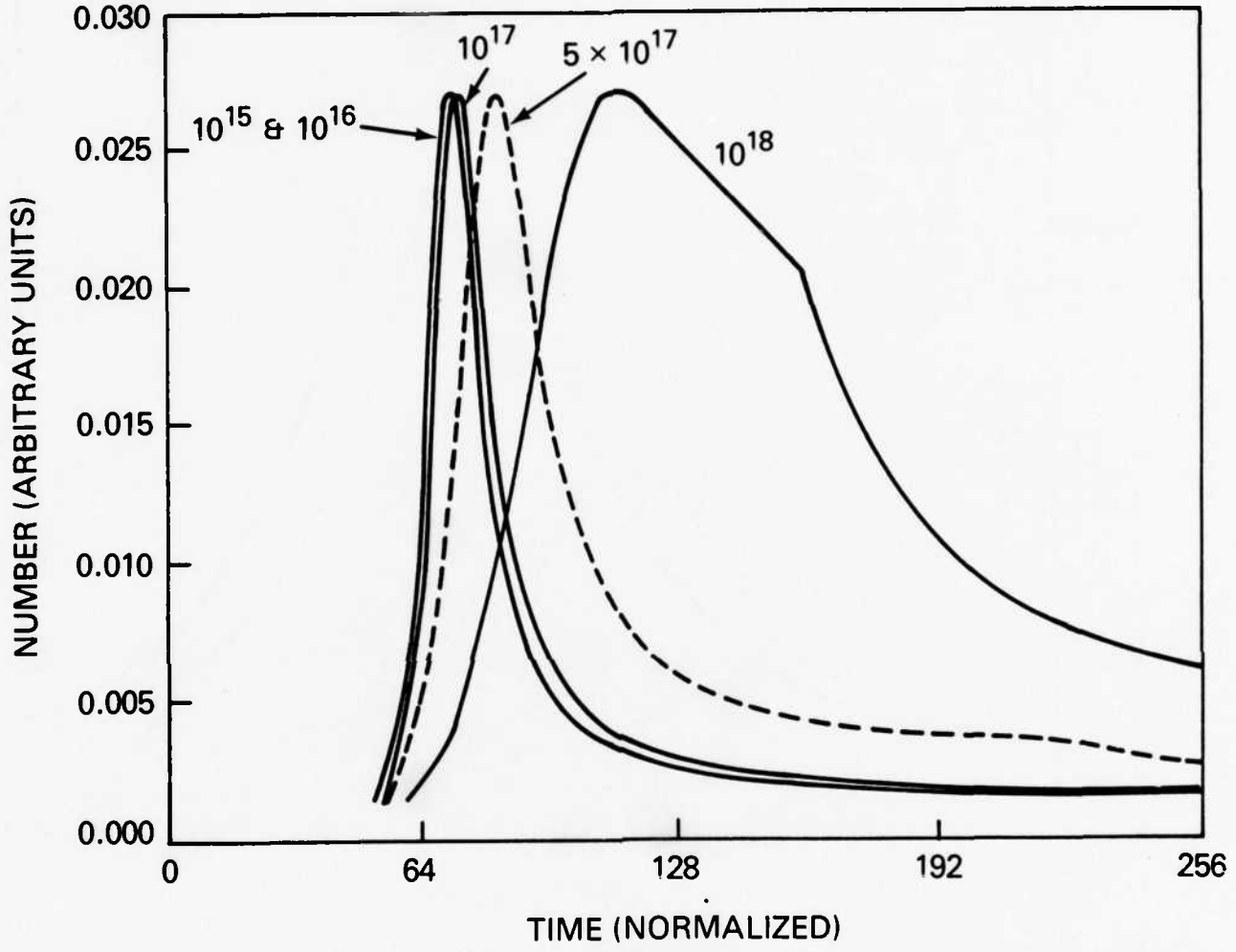

Figure 11 Distribution function of debris ions as a function of normalized time of flight (see text) for different values of F = number of molecules/cm^2 encountered by beam.

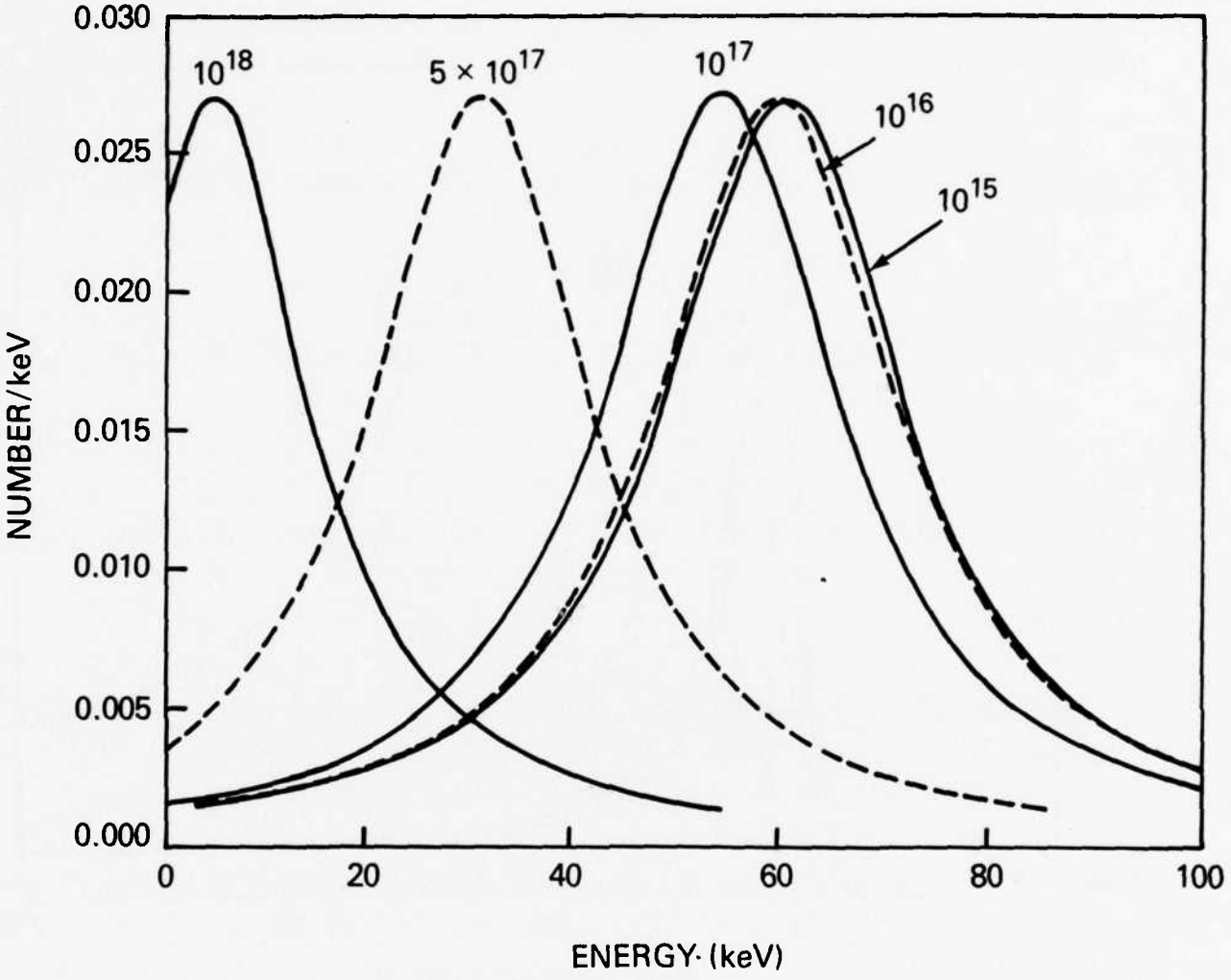

Figure 12 Energy distribution function (number/kev) of debris ions for different values of F = number of molecules/cm^2 encountered by beam.

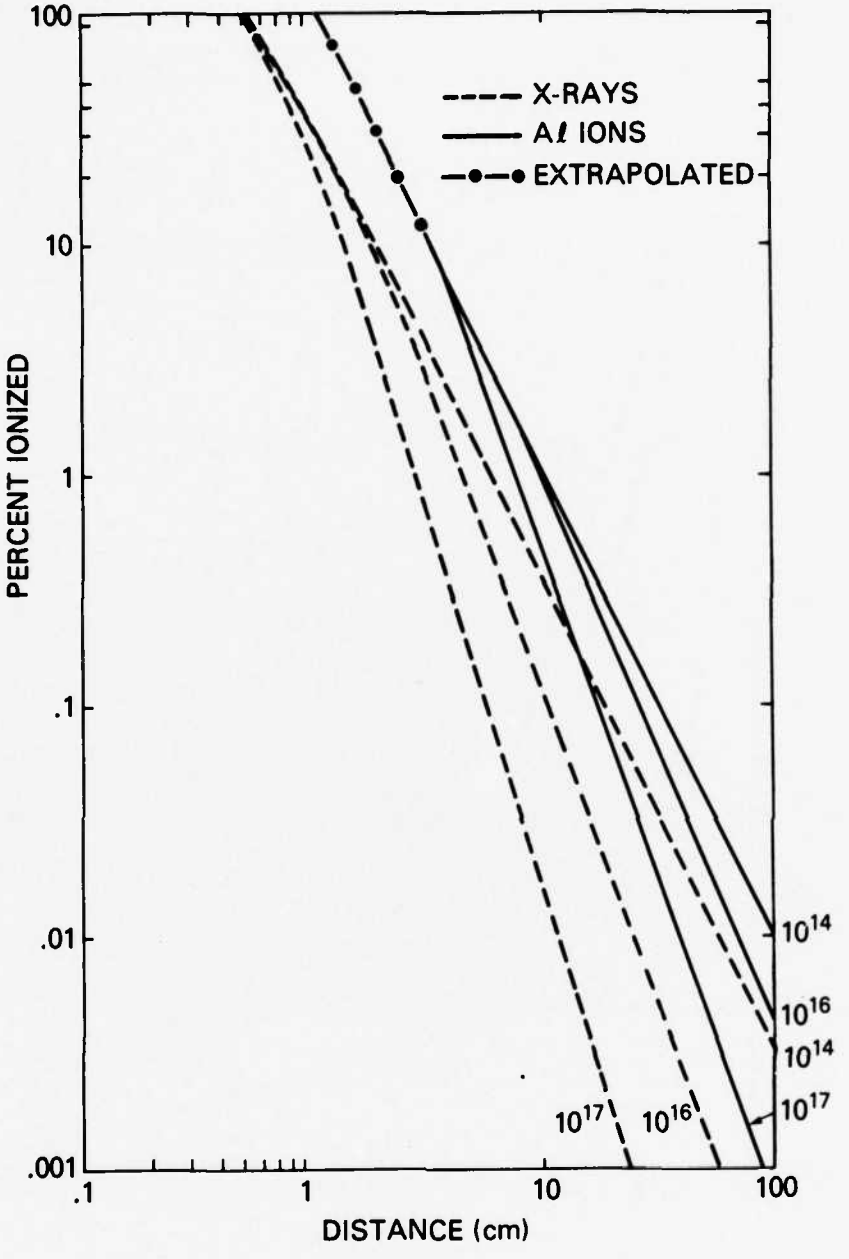

Figure 13 Percent primary ionization due to debris ions (solid curves) and x-rays (dashed curves) as a function of distance from target for various ambient N_2 densities.

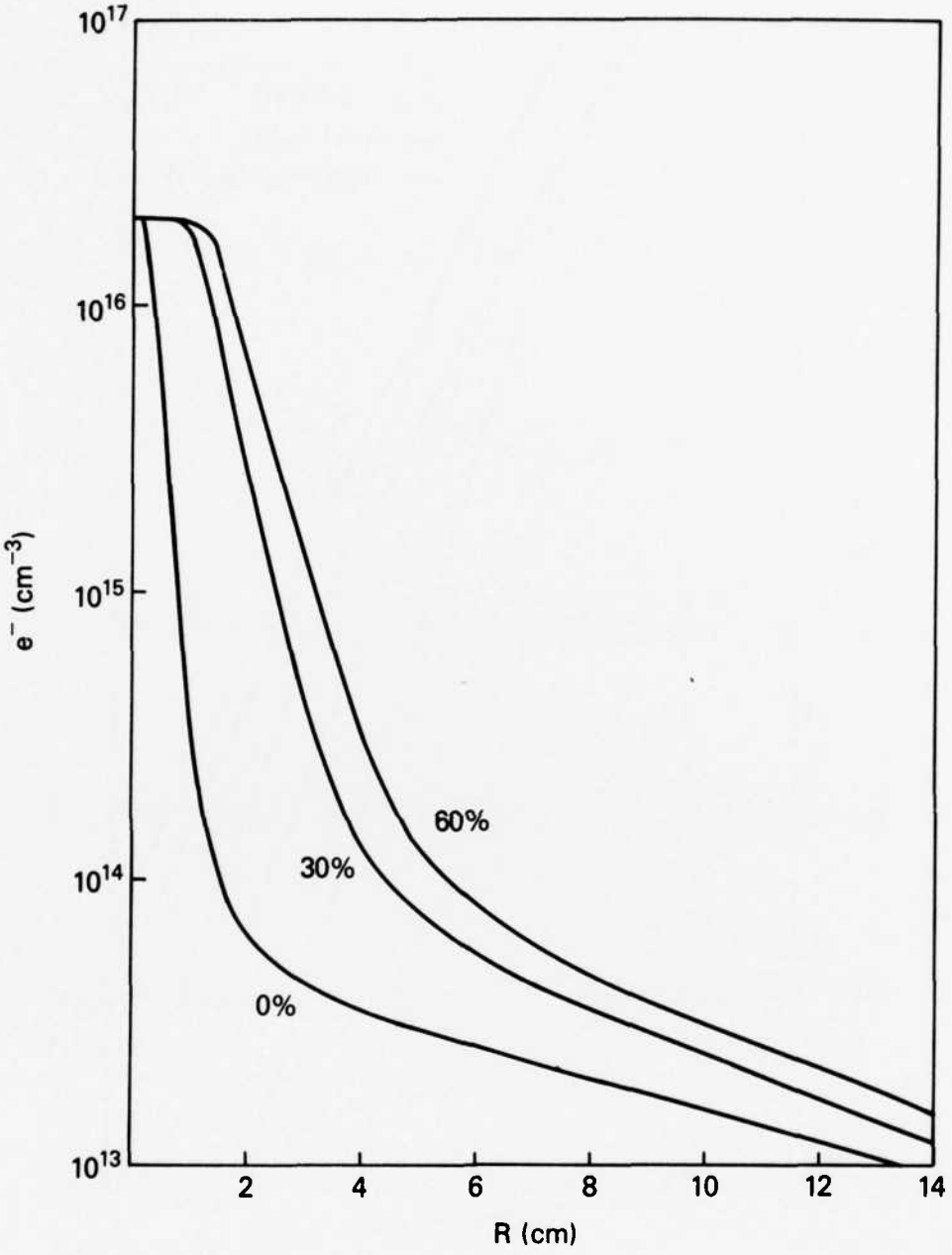

Figure 14 Electron density as a function of distance from target at approximately 5 x 10^{-7} sec after x-ray deposition. Ambient N_2 = 10^{16} cm^{-3}. Curve labels give percent of kinetic yield of debris ions converted to uv.

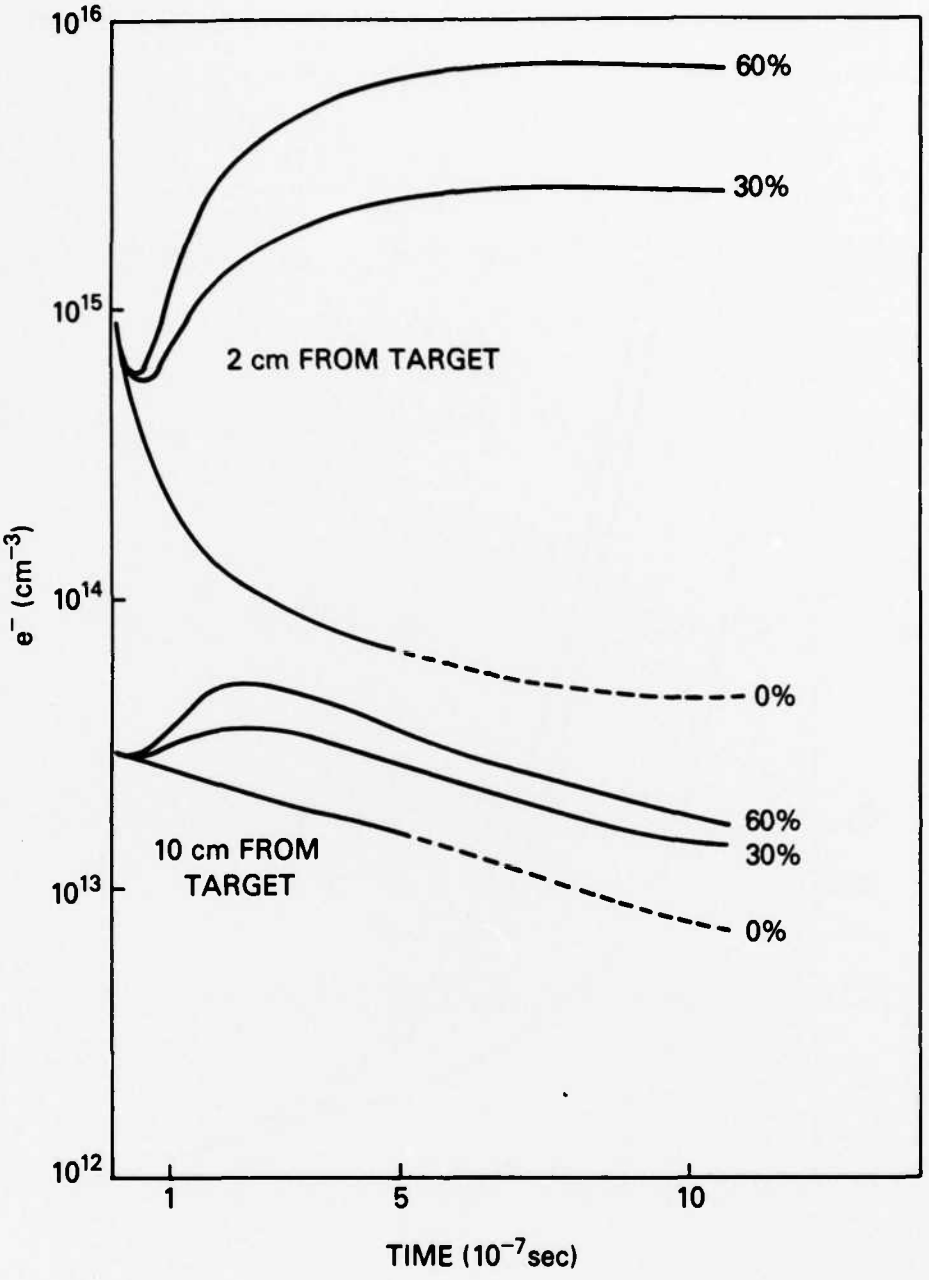

Figure 15 Electron density as a function of time after x-ray deposition at distances of 2.0 cm and 10.0 cm from target. Ambient N_2 = 10^{16} cm^{-3}. Curve labels give percent of kinetic yield of debris ions converted to uv. Dashed lines are extrapolations beyond calculation.

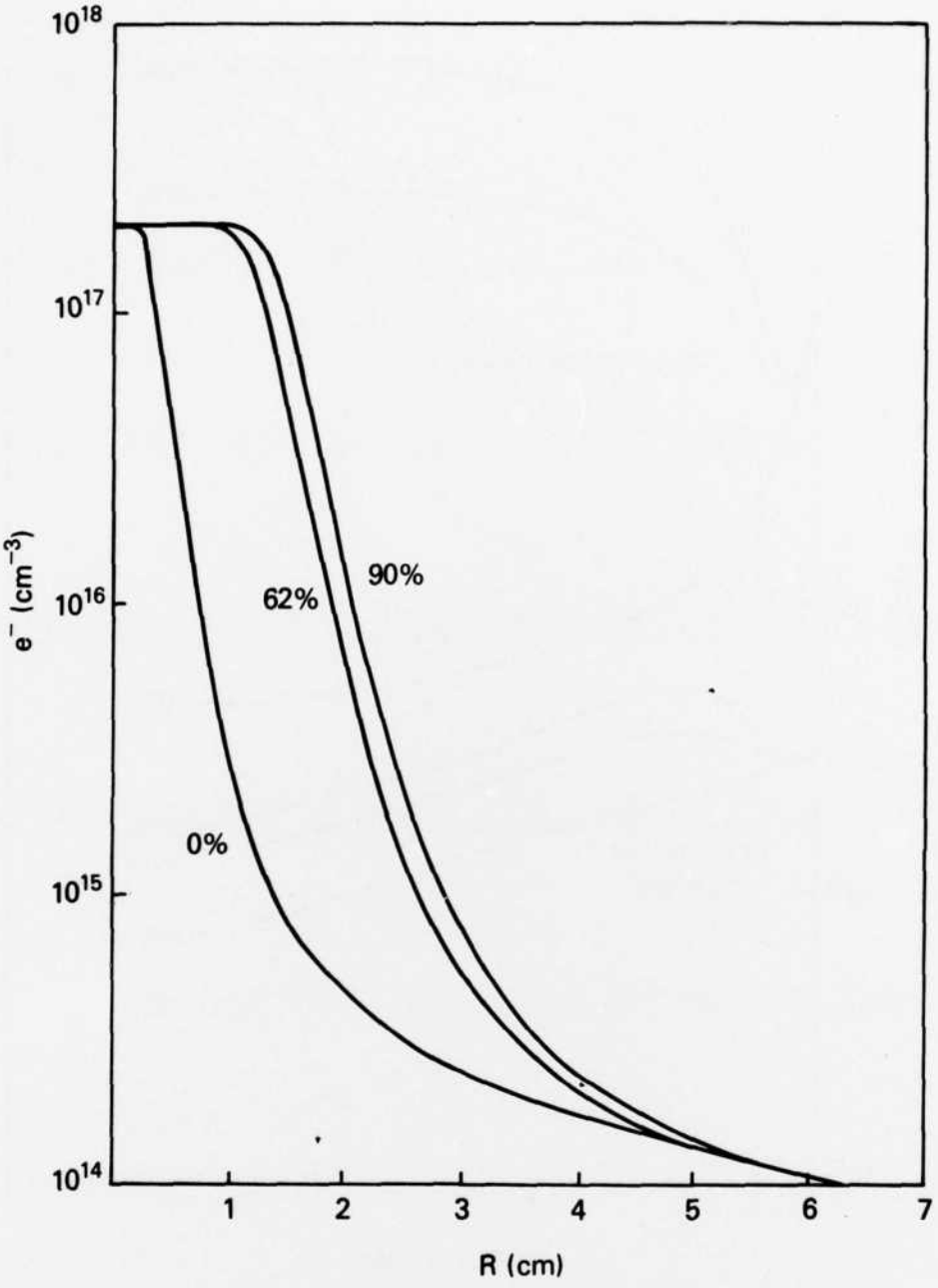

Figure 16 Electron density as a function of distance from target at approximately 1 x 10^{-7} sec after x-ray deposition. Ambient N_2 = 10^{17} cm^{-3}. Curve labels give percent of kinetic yield of debris ions converted to uv.

Acknowledgments

The authors would like to thank J. Davis, R. Clark, D. Duston, and J. Rogerson of NRL's Plasma Radiation Branch for many fruitful discussions concerning the appropriate x-ray spectrum for this experiment and aid in establishing reasonable ion-neutral cross sections. We also wish to thank B. Ripin of NRL's Laser Plasma Branch and J. Grun of Mission Research Corporation for many helpful discussions concerning the laser experiment. This work was funded by the Defense Nuclear Agency.

References

Cornwall, J.M., S. Flatté, D. Hammer, and J. Vesecky, "Studies of the effect of striations on radio communications," JASON Report JSR-81-31, 1981.

Duston, D., R.W. Clark, J. Davis, and J.P. Apruzese, "Radiation energetics of a laser-produced plasma," Phys. Rev. A, 27, 1441, 1983.

Grun, J., S.P. Obenschain, B.H. Ripin, R.R. Whitlock, E.A. McLean, J. Gardner, M.J. Herbst, and J.A. Stamper, "Ablative acceleration of planar targets to high velocities," Phys. Fluids, 26, 588, 1983.

Hyman, E., T. Young, and T. Coffey (see authors for reference), 1971.

Hyman, E., M. Mulbrandon, S.L. Ossakow, and J. Pierre, (see authors for reference), 1977.

Lampe, M., W.L. Manheimer, and K. Papadopoulos, "Anomalous transport coefficients for HANE applications due to plasma microinstabilities," NRL Memo Rept. 3076, 1975.

Longmire, C., M. Alme, R. Kilb, and L. Wright, "Scaling of debris-air coupling," MRC Report AMRC-R-338, 1981.

Rogerson, J.E. and J. Davis, "Preliminary report on a program to study proton deposition in the atmosphere," NRL Memo Rept. 2967, 1974.

Rogerson, J.E. and J. Davis, "Improved model to study proton deposition in the atmosphere," NRL Memo Report 3042, 1975.

Smith, R.A. and J.D. Huba, "Parameter survey for collisionless coupling in a laser simulation of HANE," NRL Memo Report 5092, 1983.

Sperling, J.L., "The scaling of some processes affecting structure in the high-altitude nuclear environment," JAYCOR Report J530-83-102, 1983.

Tsai, W., L.L. DeRood, Jr., and R. LeLevier, "Scaling laws for simulating early-time high-altitude nuclear explosion phenomena," R & D Associates Report RDA-TR-125003-001, 1982.

Vesecky, J.F., J.W. Chamberlain, J.M. Cornwall, D.A. Hammer, and F.W. Perkins, "Irregularities in ionospheric plasma clouds: Their evolution and effect on radio communications," JASON Report JSR-80-15, 1980.

DISTRIBUTION LIST

DEPARTMENT OF DEFENSE

ASSISTANT SECRETARY OF DEFENSE
COMM, CMD, CONT 7 INTELL
WASHINGTON, D.C. 20301

DIRECTOR
COMMAND CONTROL TECHNICAL CENTER
PENTAGON RM BE 685
WASHINGTON, D.C. 20301
01CY ATTN C-650
01CY ATTN C-312 R. MASON

DIRECTOR
DEFENSE ADVANCED RSCH PROJ AGENCY
ARCHITECT BUILDING
1400 WILSON BLVD.
ARLINGTON, VA. 22209
01CY ATTN NUCLEAR MONITORING RESEARCH
01CY ATTN STRATEGIC TECH OFFICE

DEFENSE COMMUNICATION ENGINEER CENTER
1860 WIEHLE AVENUE
RESTON, VA. 22090
01CY ATTN CODE R410
01CY ATTN CODE R812

DEFENSE TECHNICAL INFORMATION CENTER
CAMERON STATION
ALEXANDRIA, VA. 22314
02CY

DIRECTOR
DEFENSE NUCLEAR AGENCY
WASHINGTON, D.C. 20305
01CY ATTN STVL
04CY ATTN TITL
01CY ATTN DDST
03CY ATTN RAAE

COMMANDER
FIELD COMMAND
DEFENSE NUCLEAR AGENCY
KIRTLAND, AFB, NM 87115
01CY ATTN FCPR

DIRECTOR
INTERSERVICE NUCLEAR WEAPONS SCHOOL
KIRTLAND AFB, NM 87115
01CY ATTN DOCUMENT CONTROL

JOINT CHIEFS OF STAFF
WASHINGTON, D.C. 20301
01CY ATTN J-3 WWMCCS EVALUATION OFFICE

DIRECTOR
JOINT STRAT TGT PLANNING STAFF
OFFUTT AFB
OMAHA, NB 68113
01CY ATTN JLTW-2
01CY ATTN JPST G. GOETZ

CHIEF
LIVERMORE DIVISION FLD COMMAND DNA
DEPARTMENT OF DEFENSE
LAWRENCE LIVERMORE LABORATORY
P.O. BOX 808
LIVERMORE, CA 94550
01CY ATTN FCPRL

COMMANDANT
NATO SCHOOL (SHAPE)
APO NEW YORK 09172
01CY ATTN U.S. DOCUMENTS OFFICER

UNDER SECY OF DEF FOR RSCH & ENGRG
DEPARTMENT OF DEFENSE
WASHINGTON, D.C. 20301
01CY ATTN STRATEGIC & SPACE SYSTEMS (OS)

WWMCCS SYSTEM ENGINEERING ORG
WASHINGTON, D.C. 20305
01CY ATTN R. CRAWFORD

COMMANDER/DIRECTOR
ATMOSPHERIC SCIENCES LABORATORY
U.S. ARMY ELECTRONICS COMMAND
WHITE SANDS MISSILE RANGE, NM 88002
01CY ATTN DELAS-EO F. NILES

DIRECTOR
BMD ADVANCED TECH CTR
HUNTSVILLE OFFICE
P.O. BOX 1500
HUNTSVILLE, AL 35807
01CY ATTN ATC-T MELVIN T. CAPPS
01CY ATTN ATC-O W. DAVIES
01CY ATTN ATC-R DON RUSS

PROGRAM MANAGER
BMD PROGRAM OFFICE
5001 EISENHOWER AVENUE
ALEXANDRIA, VA 22333
01CY ATTN DACS-BMT J. SHEA

CHIEF C-E- SERVICES DIVISION
U.S. ARMY COMMUNICATIONS CMD
PENTAGON RM 1B269
WASHINGTON, D.C. 20310
01CY ATTN C- E-SERVICES DIVISION

COMMANDER
FRADCOM TECHNICAL SUPPORT ACTIVITY
DEPARTMENT OF THE ARMY
FORT MONMOUTH, N.J. 07703
01CY ATTN DRSEL-NL-RD H. BENNET
01CY ATTN DRSEL-PL-ENV H. BOMKE
01CY ATTN J.E. QUIGLEY

COMMANDER
U.S. ARMY COMM-ELEC ENGRG INSTAL AGY
FT. HUACHUCA, AZ 85613
01CY ATTN CCC-EMEO GEORGE LANE

COMMANDER
U.S. ARMY FOREIGN SCIENCE & TECH CTR
220 7TH STREET, NE
CHARLOTTESVILLE, VA 22901
01CY ATTN DRXST-SD

COMMANDER
U.S. ARMY MATERIAL DEV & READINESS CMD
5001 EISENHOWER AVENUE
ALEXANDRIA, VA 22333
01CY ATTN DRCLDC J.A. BENDER

COMMANDER
U.S. ARMY NUCLEAR AND CHEMICAL AGENCY
7500 BACKLICK ROAD
BLDG 2073
SPRINGFIELD, VA 22150
01CY ATTN LIBRARY

DIRECTOR
U.S. ARMY BALLISTIC RESEARCH LABORATORY
ABERDEEN PROVING GROUND, MD 21005
01CY ATTN TECH LIBRARY EDWARD BAICY

COMMANDER
U.S. ARMY SATCOM AGENCY
FT. MONMOUTH, NJ 07703
01CY ATTN DOCUMENT CONTROL

COMMANDER
U.S. ARMY MISSILE INTELLIGENCE AGENCY
REDSTONE ARSENAL, AL 35809
01CY ATTN JIM GAMBLE

DIRECTOR
U.S. ARMY TRADOC SYSTEMS ANALYSIS ACTIVITY
WHITE SANDS MISSILE RANGE, NM 88002
01CY ATTN ATAA-SA
01CY ATTN TCC/F. PAYAN JR.
01CY ATTN ATTA-TAC LTC J. HESSE

COMMANDER
NAVAL ELECTRONIC SYSTEMS COMMAND
WASHINGTON, D.C. 20360
01CY ATTN NAVALEX 034 T. HUGHES
01CY ATTN PME 117
01CY ATTN PME 117-T
01CY ATTN CODE 5011

COMMANDING OFFICER
NAVAL INTELLIGENCE SUPPORT CTR
4301 SUITLAND ROAD, BLDG. 5
WASHINGTON, D.C. 20390
01CY ATTN MR. DUBBIN STIC 12
01CY ATTN NISC-50
01CY ATTN CODE 5404 J. GALET

COMMANDER
NAVAL OCCEAN SYSTEMS CENTER
SAN DIEGO, CA 92152
01CY ATTN J. FERGUSON

NAVAL RESEARCH LABORATORY
WASHINGTON, D.C. 20375
01CY ATTN CODE 4700 S. L. Ossakow
26 CYS IF UNCLASS. 1 CY IF CLASS)
01CY ATTN CODE 4701 I Vitkovitsky
01CY ATTN CODE 4780 J. Huba (100
CYS IF UNCLASS, 1 CY IF CLASS)
01CY ATTN CODE 7500
01CY ATTN CODE 7550
01CY ATTN CODE 7580
01CY ATTN CODE 7551
01CY ATTN CODE 7555
01CY ATTN CODE 4730 E. MCLEAN
01CY ATTN CODE 4108
01CY ATTN CODE 4730 B. RIPIN
20CY ATTN CODE 2628

COMMANDER
NAVAL SEA SYSTEMS COMMAND
WASHINGTON, D.C. 20362
01CY ATTN CAPT R. PITKIN

COMMANDER
NAVAL SPACE SURVEILLANCE SYSTEM
DAHLGREN, VA 22448
01CY ATTN CAPT J.H. BURTON

OFFICER-IN-CHARGE
NAVAL SURFACE WEAPONS CENTER
WHITE OAK, SILVER SPRING, MD 20910
01CY ATTN CODE F31

DIRECTOR
STRATEGIC SYSTEMS PROJECT OFFICE
DEPARTMENT OF THE NAVY
WASHINGTON, D.C. 20376
01CY ATTN NSP-2141
01CY ATTN NSSP-2722 FRED WIMBERLY

COMMANDER
NAVAL SURFACE WEAPONS CENTER
DAHLGREN LABORATORY
DAHLGREN, VA 22448
01CY ATTN CODE DF-14 R. BUTLER

OFFICER OF NAVAL RESEARCH
ARLINGTON, VA 22217
01CY ATTN CODE 465
01CY ATTN CODE 461
01CY ATTN CODE 402
01CY ATTN CODE 420
01CY ATTN CODE 421

COMMANDER
AEROSPACE DEFENSE COMMAND/DC
DEPARTMENT OF THE AIR FORCE
ENT AFB, CO 80912
01CY ATTN DC MR. LONG

COMMANDER
AEROSPACE DEFENSE COMMAND/XPD
DEPARTMENT OF THE AIR FORCE
ENT AFB, CO 80912
01CY ATTN XPDQQ
01CY ATTN XP

AIR FORCE GEOPHYSICS LABORATORY
HANSCOM AFB, MA 01731
01CY ATTN OPR HAROLD GARDNER
01CY ATTN LKB KENNETH S.W. CHAMPION
01CY ATTN OPR ALVA T. STAIR
01CY ATTN PHD JURGEN BUCHAU
01CY ATTN PHD JOHN P. MULLEN

AF WEAPONS LABORATORY
KIRTLAND AFT, NM 87117
01CY ATTN SUL
01CY ATTN CA ARTHUR H. GUENTHER
01CY ATTN NTYCE 1LT. G. KRAJEI

AFTAC
PATRICK AFB, FL 32925
01CY ATTN TF/MAJ WILEY
01CY ATTN TN

AIR FORCE AVIONICS LABORATORY
WRIGHT-PATTERSON AFB, OH 45433
01CY ATTN AAD WADE HUNT
01CY ATTN AAD ALLEN JOHNSON

DEPUTY CHIEF OF STAFF
RESEARCH, DEVELOPMENT, & ACQ
DEPARTMENT OF THE AIR FORCE
WASHINGTON, D.C. 20330
01CY ATTN AFRDQ

HEADQUARTERS
ELECTRONIC SYSTEMS DIVISION
DEPARTMENT OF THE AIR FORCE
HANSCOM AFB, MA 01731
01CY ATTN J. DEAS

HEADQUARTERS
ELECTRONIC SYSTEMS DIVISION/YSEA
DEPARTMENT OF THE AIR FORCE
HANSCOM AFB, MA 01732
01CY ATTN YSEA

HEADQUARTERS
ELECTRONIC SYSTEMS DIVISION/DC
DEPARTMENT OF THE AIR FORCE
HANSCOM AFB, MA 01731
01CY ATTN DCKC MAJ J.C. CLARK

COMMANDER
FOREIGN TECHNOLOGY DIVISION, AFSC
WRIGHT-PATTERSON AFB, OH 45433
01CY ATTN NICD LIBRARY
01CY ATTN ETDP B. BALLARD

COMMANDER
ROME AIR DEVELOPMENT CENTER, AFSC
GRIFFISS AFB, NY 13441
01CY ATTN DOC LIBRARY/TSLD
01CY ATTN OCSE V. COYNE

SAMSO/SZ
POST OFFICE BOX 92960
WORLDWAY POSTAL CENTER
LOS ANGELES, CA 90009
(SPACE DEFENSE SYSTEMS)
01CY ATTN SZJ

STRATEGIC AIR COMMAND/XPFS
OFFUTT AFB, NB 68113
01CY ATTN ADWATE MAJ BRUCE BAUER
01CY ATTN NRT
01CY ATTN DOK CHIEF SCIENTIST

SAMSO/SK
P.O. BOX 92960
WORLDWAY POSTAL CENTER
LOS ANGELES, CA 90009
01CY ATTN SKA (SPACE COMM SYSTEMS)
M. CLAVIN

SAMSO/MN
NORTON AFB, CA 92409
(MINUTEMAN)
01CY ATTN MNNL

COMMANDER
ROME AIR DEVELOPMENT CENTER, AFSC
HANSCOM AFB, MA 01731
01CY ATTN EEP A. LORENTZEN

DEPARTMENT OF ENERGY
LIBRARY ROOM G-042
WASHINGTON, D.C. 20545
01CY ATTN DOC CON FOR A. LABOWITZ

DEPARTMENT OF ENERGY
ALBUQUERQUE OPERATIONS OFFICE
P.O. BOX 5400
ALBUQUERQUE, NM 87115
01CY ATTN DOC CON FOR D. SHERWOOD

EG&G, INC.
LOS ALAMOS DIVISION
P.O. BOX 809
LOS ALAMOS, NM 85544
01CY ATTN DOC CON FOR J. BREEDLOVE

UNIVERSITY OF CALIFORNIA
LAWRENCE LIVERMORE LABORATORY
P.O. BOX 808
LIVERMORE, CA 94550
01CY ATTN DOC CON FOR TECH INFO DEPT
01CY ATTN DOC CON FOR L-389 R. OTT
01CY ATTN DOC CON FOR L-31 R. HAGER
01CY ATTN DOC CON FOR L-46 F. SEWARD

LOS ALAMOS NATIONAL LABORATORY
P.O. BOX 1663
LOS ALAMOS, NM 87545
01CY ATTN DOC CON FOR J. WOLCOTT
01CY ATTN DOC CON FOR R.F. TASCHEK
01CY ATTN DOC CON FOR E. JONES
01CY ATTN DOC CON FOR J. MALIK
01CY ATTN DOC CON FOR R. JEFFRIES
01CY ATTN DOC CON FOR J. ZINN
01CY ATTN DOC CON FOR P. KEATON
01CY ATTN DOC CON FOR D. WESTERVELT
01CY ATTN D. SAPPENFIELD

SANDIA LABORATORIES
P.O. BOX 5800
ALBUQUERQUE, NM 87115
01CY ATTN DOC CON FOR W. BROWN
01CY ATTN DOC CON FOR A. THORNBROUGH
01CY ATTN DOC CON FOR T. WRIGHT
01CY ATTN DOC CON FOR D. DAHLGREN
01CY ATTN DOC CON FOR 3141
01CY ATTN DOC CON FOR SPACE PROJECT DIV

SANDIA LABORATORIES
LIVERMORE LABORATORY
P.O. BOX 969
LIVERMORE, CA 94550
01CY ATTN DOC CON FOR B. MURPHEY
01CY ATTN DOC CON FOR T. COOK

OFFICE OF MILITARY APPLICATION
DEPARTMENT OF ENERGY
WASHINGTON, D.C. 20545
01CY ATTN DOC CON DR. YO SONG

OTHER GOVERNMENT

DEPARTMENT OF COMMERCE
NATIONAL BUREAU OF STANDARDS
WASHINGTON, D.C. 20234
01CY (ALL CORRES: ATTN SEC OFFICER FOR)

INSTITUTE FOR TELECOM SCIENCES
NATIONAL TELECOMMUNICATIONS & INFO ADMIN
BOULDER, CO 80303
01CY ATTN A. JEAN (UNCLASS ONLY)
01CY ATTN W. UTLAUT
01CY ATTN D. CROMBIE
01CY ATTN L. BERRY

NATIONAL OCEANIC & ATMOSPHERIC ADMIN
ENVIRONMENTAL RESEARCH LABORATORIES
DEPARTMENT OF COMMERCE
BOULDER, CO 80302
01CY ATTN R. GRUBB
01CY ATTN AERONOMY LAB G. REID

DEPARTMENT OF DEFENSE CONTRACTORS

AEROSPACE CORPORATION
P.O. BOX 92957
LOS ANGELES, CA 90009
01CY ATTN I. GARFUNKEL
01CY ATTN T. SALMI
01CY ATTN V. JOSEPHSON
01CY ATTN S. BOWER
01CY ATTN D. OLSEN

ANALYTICAL SYSTEMS ENGINEERING CORP
5 OLD CONCORD ROAD
BURLINGTON, MA 01803
01CY ATTN RADIO SCIENCES

AUSTIN RESEARCH ASSOC., INC.
1901 RUTLAND DRIVE
AUSTIN, TX 78758
01CY ATTN L. SLOAN
01CY ATTN R. THOMPSON

BERKELEY RESEARCH ASSOCIATES, INC.
P.O. BOX 983
BERKELEY, CA 94701
01CY ATTN J. WORKMAN
01CY ATTN C. PRETTIE
01CY ATTN S. BRECHT

BOEING COMPANY, THE
P.O. BOX 3707
SEATTLE, WA 98124
01CY ATTN G. KEISTER
01CY ATTN D. MURRAY
01CY ATTN G. HALL
01CY ATTN J. KENNEY

CHARLES STARK DRAPER LABORATORY, INC.
555 TECHNOLOGY SQUARE
CAMBRIDGE, MA 02139
01CY ATTN D.B. COX
01CY ATTN J.P. GILMORE

COMSAT LABORATORIES
LINTHICUM ROAD
CLARKSBURG, MD 20734
01CY ATTN G. HYDE

CORNELL UNIVERSITY
DEPARTMENT OF ELECTRICAL ENGINEERING
ITHACA, NY 14850
01CY ATTN D.T. FARLEY, JR.

ELECTROSPACE SYSTEMS, INC.
BOX 1359
RICHARDSON, TX 75080
01CY ATTN H. LOGSTON
01CY ATTN SECURITY (PAUL PHILLIPS)

EOS TECHNOLOGIES, INC.
606 Wilshire Blvd.
Santa Monica, Calif 90401
01CY ATTN C.B. GABBARD

ESL, INC.
495 JAVA DRIVE
SUNNYVALE, CA 94086
01CY ATTN J. ROBERTS
01CY ATTN JAMES MARSHALL

GENERAL ELECTRIC COMPANY
SPACE DIVISION
VALLEY FORGE SPACE CENTER
GODDARD BLVD KING OF PRUSSIA
P.O. BOX 8555
PHILADELPHIA, PA 19101
01CY ATTN M.H. BORTNER SPACE SCI LAB

GENERAL ELECTRIC COMPANY
P.O. BOX 1122
SYRACUSE, NY 13201
01CY ATTN F. REIBERT

GENERAL ELECTRIC TECH SERVICES CO., INC.
HMES
COURT STREET
SYRACUSE, NY 13201
  01CY ATTN G. MILLMAN

GEOPHYSICAL INSTITUTE
UNIVERSITY OF ALASKA
FAIRBANKS, AK 99701
  (ALL CLASS ATTN: SECURITY OFFICER)
  01CY ATTN T.N. DAVIS (UNCLASS ONLY)
  01CY ATTN TECHNICAL LIBRARY
  01CY ATTN NEAL BROWN (UNCLASS ONLY)

GTE SYLVANIA, INC.
ELECTRONICS SYSTEMS GRP-EASTERN DIV
77 A STREET
NEEDHAM, MA 02194
  01CY ATTN DICK STEINHOF

HSS, INC.
2 ALFRED CIRCLE
BEDFORD, MA 01730
  01CY ATTN DONALD HANSEN

ILLINOIS, UNIVERSITY OF
107 COBLE HALL
150 DAVENPORT HOUSE
CHAMPAIGN, IL 61820
  (ALL CORRES ATTN DAN MCCLELLAND)
  01CY ATTN K. YEH

INSTITUTE FOR DEFENSE ANALYSES
1801 NO. BEAUREGARD STREET
ALEXANDRIA, VA 22311
  01CY ATTN J.M. AEIN
  01CY ATTN ERNEST BAUER
  01CY ATTN HANS WOLFARD
  01CY ATTN JOEL BENGSTON

INTL TEL & TELEGRAPH CORPORATION
500 WASHINGTON AVENUE
NUTLEY, NJ 07110
  01CY ATTN TECHNICAL LIBRARY

JAYCOR
11011 TORREYANA ROAD
P.O. BOX 85154
SAN DIEGO, CA 92138
  01CY ATTN J.L. SPERLING

JOHNS HOPKINS UNIVERSITY
APPLIED PHYSICS LABORATORY
JOHNS HOPKINS ROAD
LAUREL, MD 20810
  01CY ATTN DOCUMENT LIBRARIAN
  01CY ATTN THOMAS POTEMRA
  01CY ATTN JOHN DASSOULAS

KAMAN SCIENCES CORP
P.O. BOX 7463
COLORADO SPRINGS, CO 80933
  01CY ATTN T. MEAGHER

KAMAN TEMPO-CENTER FOR ADVANCED STUDIES
816 STATE STREET (P.O DRAWER QQ)
SANTA BARBARA, CA 93102
  01CY ATTN DASIAC
  01CY ATTN WARREN S. KNAPP
  01CY ATTN WILLIAM MCNAMARA
  01CY ATTN B. GAMBILL

LINKABIT CORP
10453 ROSELLE
SAN DIEGO, CA 92121
  01CY ATTN IRWIN JACOBS

LOCKHEED MISSILES & SPACE CO., INC
P.O. BOX 504
SUNNYVALE, CA 94088
  01CY ATTN DEPT 60-12
  01CY ATTN D.R. CHURCHILL

LOCKHEED MISSILES & SPACE CO., INC.
3251 HANOVER STREET
PALO ALTO, CA 94304
  01CY ATTN MARTIN WALT DEPT 52-12
  01CY ATTN W.L. IMHOF DEPT 52-12
  01CY ATTN RICHARD G. JOHNSON DEPT 52-12
  01CY ATTN J.B. CLADIS DEPT 52-12

MARTIN MARIETTA CORP
ORLANDO DIVISION
P.O. BOX 5837
ORLANDO, FL 32805
  01CY ATTN R. HEFFNER

M.I.T. LINCOLN LABORATORY
P.O. BOX 73
LEXINGTON, MA 02173
  01CY ATTN DAVID M. TOWLE
  01CY ATTN L. LOUGHLIN
  01CY ATTN D. CLARK

MCDONNEL DOUGLAS CORPORATION
5301 BOLSA AVENUE
HUNTINGTON BEACH, CA 92647
01CY ATTN N. HARRIS
01CY ATTN J. MOULE
01CY ATTN GEORGE MROZ
01CY ATTN W. OLSON
01CY ATTN R.W. HALPRIN
01CY ATTN TECHNICAL LIBRARY SERVICES

MISSION RESEARCH CORPORATION
735 STATE STREET
SANTA BARBARA, CA 93101
01CY ATTN P. FISCHER
01CY ATTN W.F. CREVIER
01CY ATTN STEVEN L. GUTSCHE
01CY ATTN R. BOGUSCH
01CY ATTN R. HENDRICK
01CY ATTN RALPH KILB
01CY ATTN DAVE SOWLE
01CY ATTN F. FAJEN
01CY ATTN M. SCHEIBE
01CY ATTN CONRAD L. LONGMIRE
01CY ATTN B. WHITE

MISSION RESEARCH CORP.
1400 SAN MATEO BLVD. SE
SUITE A
ALBUQUERQUE, NEW MEXICO 87108
01CY R. STELLINGWERF
01CY M. ALME
01CY L. WRIGHT

MITRE CORPORATION, THE
P.O. BOX 208
BEDFORD, MA 01730
01CY ATTN JOHN MORGANSTERN
01CY ATTN G. HARDING
01CY ATTN C.E. CALLAHAN

MITRE CORP
WESTGATE RESEARCH PARK
1820 DOLLY MADISON BLVD
MCLEAN, VA 22101
01CY ATTN W. HALL
01CY ATTN W. FOSTER

PACIFIC-SIERRA RESEARCH CORP
12340 SANTA MONICA BLVD.
LOS ANGELES, CA 90025
01CY ATTN E.C. FIELD, JR.

PENNSYLVANIA STATE UNIVERSITY
IONOSPHERE RESEARCH LAB
318 ELECTRICAL ENGINEERING EAST
UNIVERSITY PARK, PA 16802
(NO CLASS TO THIS ADDRESS)
01CY ATTN IONOSPHERIC RESEARCH LAB

PHOTOMETRICS, INC.
4 ARROW DRIVE
WOBURN, MA 01801
01CY ATTN IRVING L. KOFSKY

PHYSICAL DYNAMICS, INC.
P.O. BOX 3027
BELLEVUE, WA 98009
01CY ATTN E.J. FREMOUW

PHYSICAL DYNAMICS, INC.
P.O. BOX 10367
OAKLAND, CA 94610
ATTN A. THOMSON

R & D ASSOCIATES
P.O. BOX 9695
MARINA DEL REY, CA 90291
01CY ATTN FORREST GILMORE
01CY ATTN WILLIAM B. WRIGHT, JR.
01CY ATTN ROBERT F. LELEVIER
01CY ATTN WILLIAM J. KARZAS
01CY ATTN H. ORY
01CY ATTN C. MACDONALD
01CY ATTN R. TURCO
01CY ATTN L. DeRAND
01CY ATTN W. TSAI

RAND CORPORATION, THE
1700 MAIN STREET
SANTA MONICA, CA 90406
01CY ATTN CULLEN CRAIN
01CY ATTN ED BEDROZIAN

RAYTHEON CO.
528 BOSTON POST ROAD
SUDBURY, MA 01776
01CY ATTN BARBARA ADAMS

RIVERSIDE RESEARCH INSTITUTE
80 WEST END AVENUE
NEW YORK, NY 10023
01CY ATTN VINCE TRAPANI

SCIENCE APPLICATIONS, INC.
P.O. BOX 2351
LA JOLLA, CA 92038
01CY ATTN LEWIS M. LINSON
01CY ATTN DANIEL A. HAMLIN
01CY ATTN E. FRIEMAN
01CY ATTN E.A. STRAKER
01CY ATTN CURTIS A. SMITH
01CY ATTN JACK MCDOUGALL

SCIENCE APPLICATIONS, INC
1710 GOODRIDGE DR.
MCLEAN, VA 22102
ATTN: J. COCKAYNE

SRI INTERNATIONAL
333 RAVENSWOOD AVENUE
MENLO PARK, CA 94025
01CY ATTN DONALD NEILSON
01CY ATTN ALAN BURNS
01CY ATTN G. SMITH
01CY ATTN R. TSUNODA
01CY ATTN DAVID A. JOHNSON
01CY ATTN WALTER G. CHESNUT
01CY ATTN CHARLES L. RINO
01CY ATTN WALTER JAYE
01CY ATTN J. VICKREY
01CY ATTN RAY L. LEADABRAND
01CY ATTN G. CARPENTER
01CY ATTN G. PRICE
01CY ATTN R. LIVINGSTON
01CY ATTN V. GONZALES
01CY ATTN D. MCDANIEL

TECHNOLOGY INTERNATIONAL CORP
75 WIGGINS AVENUE
BEDFORD, MA 01730
01CY ATTN W.P. BOQUIST

TOYON RESEARCH CO.
P.O. Box 6890
SANTA BARBARA, CA 93111
01CY ATTN JOHN ISE, JR.
01CY ATTN JOEL GARBARINO

TRW DEFENSE & SPACE SYS GROUP
ONE SPACE PARK
REDONDO BEACH, CA 90278
01CY ATTN R. K. PLEBUCH
01CY ATTN S. ALTSCHULER
01CY ATTN D. DEE
01CY ATTN D/ STOCKWELL
SNTF/1575

VISIDYNE
SOUTH BEDFORD STREET
BURLINGTON, MASS 01803
01CY ATTN W. REIDY
01CY ATTN J. CARPENTER
01CY ATTN C. HUMPHREY

IONOSPHERIC MODELING DISTRIBUTION LIST
(UNCLASSIFIED ONLY)

PLEASE DISTRIBUTE ONE COPY TO EACH OF THE FOLLOWING PEOPLE (UNLESS OTHERWISE NOTED)

NAVAL RESEARCH LABORATORY
WASHINGTON, D.C. 20375
- DR. S. OSSAKOW - Code 4700 (26 Copies)
- Code 4701
- Code 4780 (100 copies)
- DR. P. MANGE - CODE 4101
- DR. E. SZUSZCZEWICZ - CODE 4108
- DR. J. GOODMAN - CODE 4180
- DR. P. RODRIGUEZ - CODE 4108

A.F. GEOPHYSICS LABORATORY
L.G. HANSCOM FIELD
BEDFORD, MA 01730
- DR. T. ELKINS
- DR. W. SWIDER
- MRS. R. SAGALYN
- DR. J.M. FORBES
- DR. T J. KENESHEA
- DR. w. BURKE
- DR. H. CARLSON
- DR. J. JASPERSE

BOSTON UNIVERSITY
DEPARTMENT OF ASTRONOMY
BOSTON, MA 02215
- DR. J. AARONS

CORNELL UNIVERSITY
ITHACA, NY 14850
- DR. W.E. SWARTZ
- DR. R. SUDAN
- DR. D. FARLEY
- DR. M. KELLEY

HARVARD UNIVERSITY
HARVARD SQUARE
CAMBRIDGE, MA 02138
- DR. M.B. McELROY
- DR. R. LINDZEN

INSTITUTE FOR DEFENSE ANALYSIS
400 ARMY/NAVY DRIVE
ARLINGTON, VA 22202
- DR. E. BAUER

MASSACHUSETTS INSTITUTE OF TECHNOLOGY
PLASMA FUSION CENTER
LIBRARY, NW16-262
CAMBRIDGE, MA 02139

NASA
GODDARD SPACE FLIGHT CENTER
GREENBELT, MD 20771
- DR. R.F. BENSON
- DR. K. MAEDA
- Dr. S. CURTIS
- Dr. M. DUBIN
- DR. N. MAYNARD - CODE 696

COMMANDER
NAVAL AIR SYSTEMS COMMAND
DEPARTMENT OF THE NAVY
WASHINGTON, D.C. 20360
- DR. T. CZUBA

COMMANDER
NAVAL OCEAN SYSTEMS CENTER
SAN DIEGO. CA 92152
- MR. R. ROSE - CODE 5321

NOAA
DIRECTOR OF SPACE AND ENVIRONMENTAL LABORATORY
BOULDER, CO 80302
- DR. A. GLENN JEAN
- DR. G.W. ADAMS
- DR. D.N. ANDERSON
- DR. K. DAVIES
- DR. R. F. DONNELLY

OFFICE OF NAVAL RESEARCH
800 NORTH QUINCY STREET
ARLINGTON, VA 22217
- DR. G. JOINER

PENNSYLVANIA STATE UNIVERSITY
UNIVERSITY PARK, PA 16802
DR. J.S. NISBET
DR. P.R. ROHRBAUGH
DR. L.A. CARPENTER
DR. M. LEE
DR. R. DIVANY
DR. P. BENNETT
DR. F. KLEVANS

PRINCETON UNIVERSITY
PLASMA PHYSICS LABORATORY
PRINCETON, NJ 08540
DR. F. PERKINS

SCIENCE APPLICATIONS, INC.
1150 PROSPECT PLAZA
LA JOLLA, CA 92037
DR. D.A. HAMLIN
DR. L. LINSON
DR. E. FRIEMAN

STANFORD UNIVERSITY
STANFORD, CA 94305
DR. P.M. BANKS

U.S. ARMY ABERDEEN RESEARCH
AND DEVELOPMENT CENTER
BALLISTIC RESEARCH LABORATORY
ABERDEEN, MD
DR. J. HEIMERL

GEOPHYSICAL INSTITUTE
UNIVERSITY OF ALASKA
FAIRBANKS, AK 99701
DR. L.C. LEE

UNIVERSITY OF CALIFORNIA,
BERKELEY
BERKELEY, CA 94720
DR. M. HUDSON

UNIVERSITY OF CALIFORNIA
LOS ALAMOS SCIENTIFIC LABORATORY
J-10, MS-664
LOS ALAMOS, NM 87545
DR. M. PONGRATZ
DR. D. SIMONS
DR. G. BARASCH
DR. L. DUNCAN
DR. P. BERNHARDT
DR. S.P. GARY

UNIVERSITY OF CALIFORNIA,
LOS ANGELES
405 HILLGARD AVENUE
LOS ANGELES, CA 90024
DR. F.V. CORONITI
DR. C. KENNEL
DR. A.Y. WONG

UNIVERSITY OF MARYLAND
COLLEGE PARK, MD 20740
DR. K. PAPADOPOULOS
DR. E. OTT

JOHNS HOPKINS UNIVERSITY
APPLIED PHYSICS LABORATORY
JOHNS HOPKINS ROAD
LAUREL, MD 20810
DR. R. GREENWALD
DR. C. MENG

UNIVERSITY OF PITTSBURGH
PITTSBURGH, PA 15213
DR. N. ZABUSKY
DR. M. BIONDI
DR. E. OVERMAN

UNIVERSITY OF TEXAS
AT DALLAS
CENTER FOR SPACE SCIENCES
P.O. BOX 688
RICHARDSON, TEXAS 75080
DR. R. HEELIS
DR. W. HANSON
DR. J.P. McCLURE

UTAH STATE UNIVERSITY
4TH AND 8TH STREETS
LOGAN, UTAH 84322
DR. R. HARRIS
DR. K. BAKER
DR. R. SCHUNK
DR. J. ST.-MAURICE

PHYSICAL RESEARCH LABORATORY
PLASMA PHYSICS PROGRAMME
AHMEDABAD 380 009
INDIA
P.J. PATHAK, LIBRARIAN

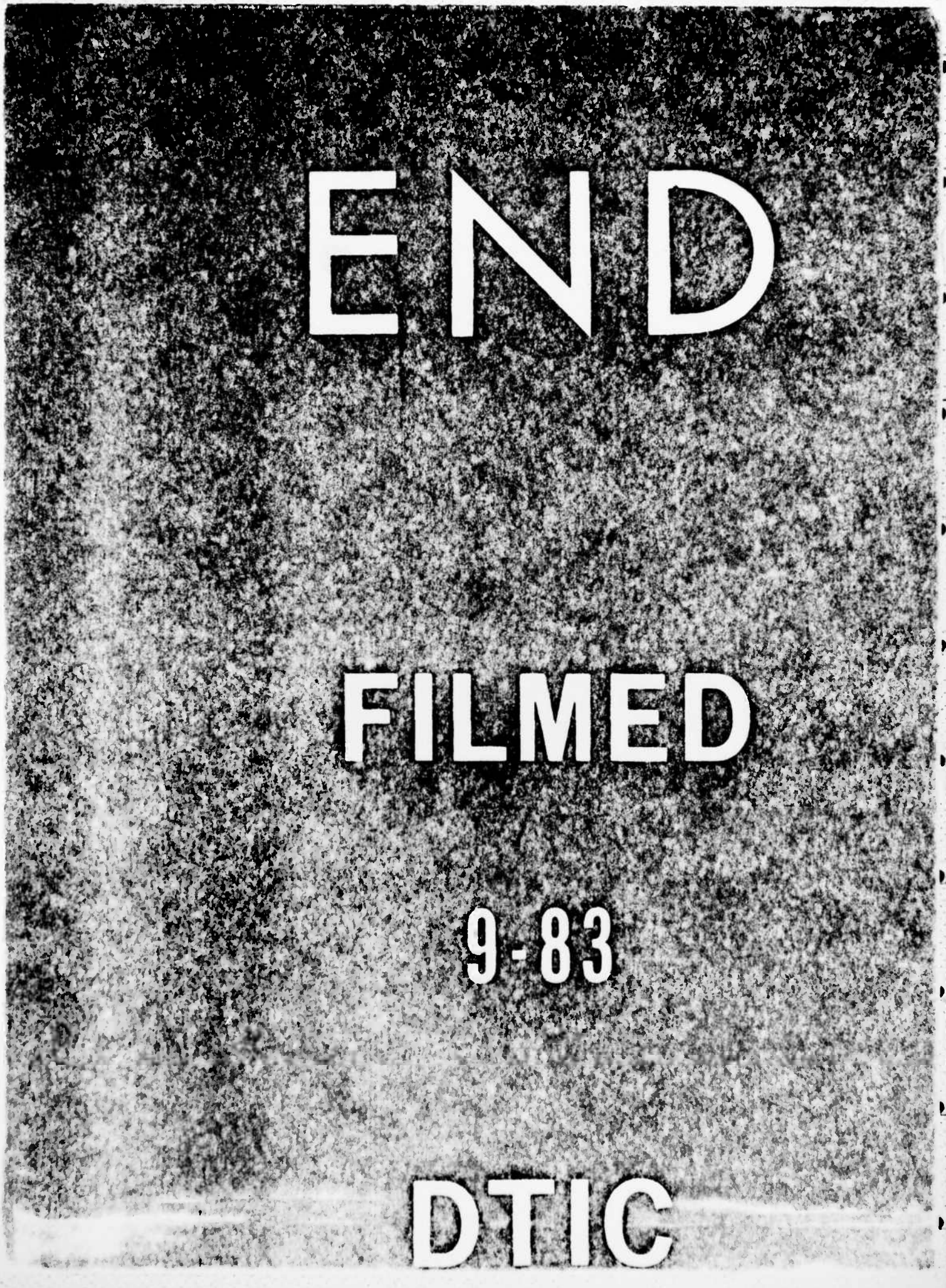
END
FILMED
9-83
DTIC